European Journal of Mechanics / B Fluids 108 (2024) 104–118

Contents lists available at ScienceDirect

European Journal of Mechanics / B Fluids

journal homepage: www.elsevier.com/locate/ejmflu

Dynamics and applications of finite-size fibre-like objects in turbulent flows

Alessandro Chiarini [a], Marco Edoardo Rosti [a,*], Andrea Mazzino [b,c]

[a] Complex Fluids and Flows Unit, Okinawa Institute of Science and Technology Graduate University (OIST), 1919-1 Tancha, Onna-son, Okinawa 904-0495, Japan
[b] Department of Civil, Chemical and Environmental Engineering, Via Montallegro 1, Genova, 16145, Italy
[c] INFN, Instituto Nazionale di Fisica Nucleare, Sezione di Genova, Via Dodecaneso 33, Genova, 16146, Italy

ARTICLE INFO

Keywords:
Fibre-laden turbulent flows
Multiphase flows

ABSTRACT

This review delves into the dynamics of fibre-laden turbulent flows, a field that has garnered substantial attention due to its relevance in both natural and engineering contexts. The focus here is mainly on finite-size fibres, those exceeding the Kolmogorov scale, diverging from the commonly studied smaller ones. The study synthesises current understanding of the behaviour and organisation of both rigid and flexible finite-size fibres within turbulent flows, underscoring the added complexity these anisotropic particles introduce compared to their spherical counterparts. The influence of the length, the curvature and the inertia on the dynamics of rigid and flexible fibres is addressed. Fibre-based novel experimental methods, such as Fibre Tracking Velocimetry, are highlighted. Ultimately, this paper seeks to provide a clearer picture of the intricate dynamics at play in fibre-laden turbulent flows and their practical implications in various fields.

1. Introduction

Turbulent flows laden with fibre-like objects have been the focus of many studies over the last years, since suspension of anisotropic objects in turbulent flows are often encountered in several natural environments and engineering applications [1–3]. Few examples are microplastics or non-motile microorganisms in aquatic environments [4], marine litter in the ocean [5,6], locomotion of bacteria or planktonic organisms [7], the formation of algae aggregates [8], and the pulp production in papermaking [9,10]. However, the fluid–structure interaction mechanisms between fibres and the fluid's degrees of freedom are non-trivial even in the context of laminar flows. The role of fibres in enhancing swimming/flying organism locomotion efficiency through spontaneous symmetry breaking and resonance [11–13] phenomena is just one relevant example underscoring their critical contribution to the dynamic interaction between organisms and their fluid environments.

Compared to the more studied spherical particles [14,15], the anisotropic character of fibre-like objects gives additional complexity to their interaction with the flow. Already in the idealised case of rigid fibres, these objects show some peculiar features, such as preferential alignment with some properties of the flow like vorticity or strain rate principal directions [16], and a complex motion characterised by tumbling and spinning [17–19]. This further complicates the interaction between the fluid and the solid phase, and the scenario becomes even more intricate in the case of flexible fibres; in this case the suspended fibres have many degrees of freedom in deformation, and can even exhibit instabilities [3].

From the numerical point of view, over the years a large number of studies has focused on the dynamics of the dispersed phase assuming that the suspension is dilute enough, so that the backreaction of the solid phase to the carrier fluid can be safely neglected. Based on these hypothesis, one-way coupling approaches (i.e. the fluid is not affected by the presence of the solid phase) are used and the problem is largely simplified. In case of rigid particles with ellipsoidal shape that are sufficiently small to be modelled as evolving in a Stokes flow, Jeffery and Filon [20] derived an analytical expression for the fluid torque acting on the particle. This expression has been later generalised to other shapes, and has been largely exploited for a large variety of problems, including studies on the rheology of suspensions in low Reynolds number conditions [21], and on the dynamics of dispersed fibres in turbulent flows [16].

Despite the relevance of these studies, the approaches based on the Jeffrey's solution are justified only under the strict assumption of small and rigid objects. The Stokes approximation, indeed, holds only when the particle Reynolds number is very low and the flow around the particle is smooth. Moreover, when considering relatively high concentrations of fibres, one has to consider the two-way coupled problem: the fibres are transported (and potentially deformed) by the flow and, in turn, they modify the surrounding flow due to the no-slip condition at their surface [14,15]. In this sense, large steps towards a comprehensive understanding of the complex interaction between rigid/flexible fibres and the fluid phase have been performed thanks to

* Corresponding author.
E-mail address: marco.rosti@oist.jp (M.E. Rosti).

https://doi.org/10.1016/j.euromechflu.2024.07.007
Received 23 February 2024; Received in revised form 21 May 2024; Accepted 6 July 2024
Available online 11 July 2024

the increase of the supercomputer's power, which enables to resolve the flow around each object by means of suitable techniques, e.g. immersed boundary methods [22–26]. Also, in many applications fibres are flexible. In this case, the way they interact with the flow is not trivial and requires a more complex modelling approach as they may experience large deformations, and force the flow at their characteristic scales and frequencies. For small fibres the most common modelling approach relies on the slender body theory; see for example the work by Olivieri et al. [27] and the works by Young and Shelley [28], Wandersman et al. [29], Quennouz et al. [30], which show that the dynamics of the fibres is largely influenced by the flow-induced buckling instabilities.

The flow modulation by solid/flexible non spherical objects in non-dilute conditions has started to be studied over the last few years [see for example [27] and references therein]. When the concentration of the fibres is large enough the flow shows a substantial departure from the classical phenomenology observed for a purely Newtonian fluid. In homogeneous isotropic turbulence, for example, the presence of the solid phase interacts with the classical energy cascade and modifies the scale-by-scale energy redistribution [31]. In turbulent channels, instead, the presence of non spherical objects modifies the mean flow and the organisation of the near-wall velocity fluctuations, potentially leading to a reduction of the friction drag [23].

From a complementary perspective, recent studies have focused on the possibility of exploiting fibre-like objects to measure the properties of turbulent flows [25,32–34]. Rosti et al. [32] and Rosti et al. [34] considered flexible fibres and found that they present a different flapping motion depending on their flexibility. They observed that in some regimes, fibres may behave as a proxy of turbulent eddies of comparable size, and enable the measurement of two-point flow statistics, by simply tracking the motion of the end-to-end fibres. Following the seminal work by Cavaiola et al. [25], Brizzolara et al. [35] introduced a novel experimental technique, named "Fibre Tracking Velocimetry", which measures the properties of turbulence at a fixed length scale, by following the translation and rotation of rigid fibres, extending already existing techniques based on particle tracers.

The aim of this contribution is to review the last progresses on turbulent flows laden with fibre-like objects. This review comes after the works by Voth and Soldati [16] and du Roure et al. [3], which have mainly considered small fibres. To differentiate, here we mainly focus on finite-size fibre-like objects, i.e. anisotropic particles with size larger than the Kolmogorov scale. Some works dealing with sub-Kolmogorov fibres are however considered for comparison purposes. The specific objectives of this work are: (i) to briefly describe how finite-size fibre-like objects behave in a turbulent flow and how they are distributed, focusing on the effect of their length, shape and inertia, and (ii) to review how solid/flexible fibre-like objects can be used as tools to control the flow, or to extract flow features.

2. How are fibre-like objects organised in turbulent flows?

2.1. Rigid objects

The dynamics of anisotropic particles moving within a flow is rich and complicated. Depending on their size and inertia, these particles may rotate, tumble, spin, and preferentially locate themselves in specific regions of the flow. The term 'tumbling' denotes the orientational dynamics of the particles' symmetry axis, while 'spinning' refers to the rotation of the particles around their own symmetry axis; see Fig. 1. Anisotropic particles have a preferential direction that influences their alignment, their overall dynamics, and their ability to cluster in particular regions of the flow.

In the case of rigid particles with ellipsoidal shape and which are sufficiently small to be considered to evolve in a Stokes flow, an analytical expression for the fluid torque acting on the particle was originally derived by Jeffery and Filon [20]. This formulation has been then generalised to other shapes and widely exploited in a variety of problems to characterise the rheology of suspensions [see e.g. [21]]. Several works have indeed used this model to characterise the dynamics of small dispersed fibres in turbulent flows [see [16] and references therein]. However, the approach based on Jeffery's solution does not apply if the Reynolds number at the fibre length scale is not sufficiently small or if the flow surrounding the fibres is not smooth. The dynamical behaviour of fibres with length well within the inertial range of scales, in fact, is far less understood and has only recently been considered by a few experimental [e.g., [17,19,36]] and numerical [e.g., [22]] studies.

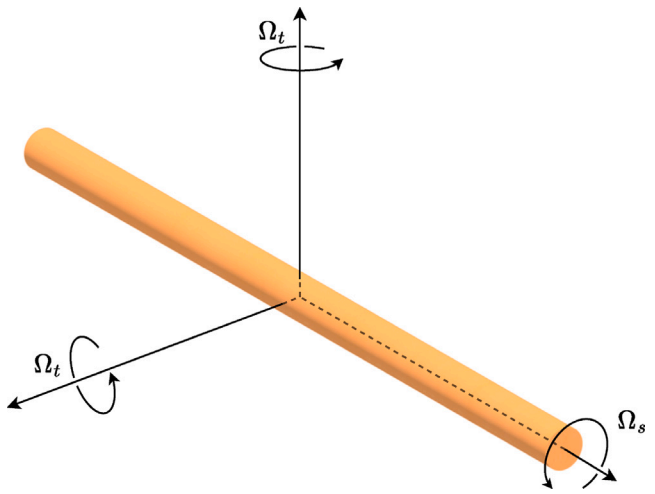

Fig. 1. Sketch of an anisotropic particle. Ω_s refer to the spinning rotation rate, i.e. the component of the rotation rate around the symmetry axis. Ω_t refer to the tumbling rotation rate, i.e the component of the rotation rate perpendicular to the symmetry axis.

2.1.1. Homogeneous isotropic turbulence

The translational and rotational motion of rigid fibres in turbulent flows depends on their shape and length, and on the ratio between their characteristic length and that of the flow. This problem has been extensively studied by Shin and Koch [37]. They performed direct numerical simulations to study the motion of fibres in homogeneous isotropic turbulence. They used the slender-body theory [38] on neutrally buoyant fibres, and solved the fluid–structure interaction problem by dividing the flow region around a single fibre in inner and outer region by means of an asymptotic expansion (see their paper for more details). They varied the length of the fibres in the $0.3 \leq L/\eta \leq 59$ range (η is the Kolmogorov scale) to consider fibres smaller and larger than the Kolmogorov scale. They observed that fibres with $L \ll \eta$ translate like fluid particles and rotate like fluid material lines [39]. The fibre acceleration a variance matches the acceleration variance of a fluid particle, and the fibres rotation rate depends on the local velocity derivatives (see Fig. 2). When the fibres length increases, instead, their motion does not follow the local properties of the flow. Their translational and rotational motions slow down, as the fibres become more insensitive to the fast small-scale eddies. This results into a decrease of the fibre acceleration and rotation-rate variances (see Fig. 2).

Parsa et al. [41] report the first three-dimensional experimental measurements of the orientation dynamics of small rodlike particles in a turbulent flow. In their study they considered small ellipsoidal particles with length of $L = 2.6\eta$ and $L = 4.8\eta$, and observed how the rotation rate changes with the aspect ratio $\lambda = L/d$ of the ellipsoid; d is the minor length of the particles. They observed a quite good agreement of their experimental results with the model of Jeffery and Filon [20]. The only discrepancy they found was associated with the tails of the probability density function of the squared rotation rate, suggesting that the finite size of the fibres influences only the rare

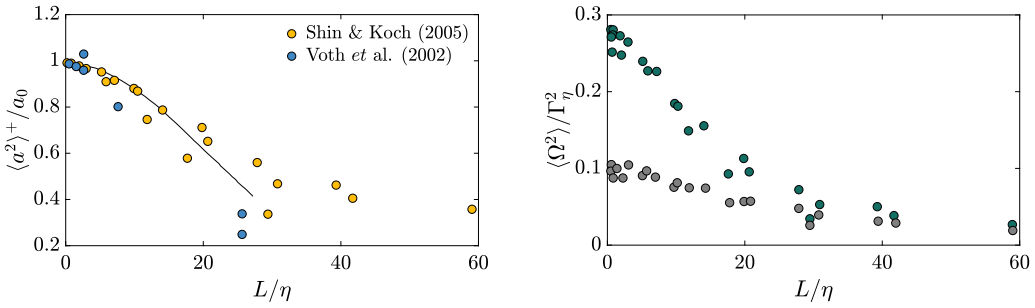

Fig. 2. Left: the fibre acceleration a variance normalised with the acceleration variance of a fluid particle as a function of the fibre length L. The orange circles are from the direct numerical simulations of [37] and refer to different Re_λ. The blue symbols denote experimental data for spherical particles with diameter L, from [40]. Right: variances of the fibre rotation rate as a function of the fibre length. Γ_η is the Kolmogorov shear rate. Green and grey circles denote results for the initial and long-time (after the fibre orientation has become correlated with the turbulent flow) variances respectively. $\Gamma_\eta = (\epsilon/\nu)^{1/2}$ is the Kolmogorov shear rate. (For interpretation of the references to colour in this figure legend, the reader is referred to the web version of this article.)
Source: Adapted from [37].

but intense events for $L/\eta \lessapprox 5$. Tracking the motion of the fibres, they observed that their rotation rate does not increase when fibres are caught in a vortex, since they align with the vorticity. This reflects the tendency of anisotropic particles to become aligned with the velocity gradients of the flow. They also found that the mean square rotation rate of elongated fibres with $\lambda \gg 1$ immersed in a turbulent flow is much smaller than that of randomly oriented fibres. This is because the alignment of the fibres with the vorticity reduces the variance of the rotation rate, as only the vorticity perpendicular to the fibres contribute to their rotation rate. They also found that for anisotropic particles the probability density function of the square rotation rate has larger tails compared to spherical particles. In fact, a small variation of the orientation of the fibres with respect to the velocity gradient tensor contribute to additional large fluctuations, resulting to high rotation rate events. Later, Chevillard and Meneveau [42] numerically generalised the work of Parsa et al. [41] and considered the orientation dynamics and rotation rate of general triaxial–ellipsoidal particles, i.e. particles with major semi-axis of length d_1, d_2 and d_3 with $d_1 \neq d_2 \neq d_3$, in homogeneous isotropic turbulence. However, they considered a generalisation of Jeffery's equations reported in Junk and Illner [43] and, thus, their analysis is valid only for particles that are smaller than the Kolmogorov scale. They found that triaxial ellipsoids that are very long in one direction, very thin in another and of intermediate size in the third one, exhibit reduced rotation rates around the major axis, like for rods. In contrast, they exhibit increased rotating rates in the direction with the smallest thickness, like for axisymmetric discs.

The dependence of the rotation of anisotropic particles on their shape has been investigated by Byron et al. [44]. They considered cylinders and spheroids, i.e. shapes that are characterised by an axis of symmetry and two other axes of equal lengths. The authors used both numerical and analytical calculations based on the Jeffery's approximation, and laboratory experiments. They considered particles with size that ranges between the dissipative and the inertial subrange of turbulence, with $L > \eta$.

The experiments validate their numerical simulations, meaning that the dependence of the particles' rotation on their shape does not change with the particle size. They observed that the symmetry axis of the rods follows closely the second strain eigenvector $\boldsymbol{e}_2$ and vorticity, while the symmetry axis of the discs tumbles in the plane spanned by the strain eigenvectors, $\boldsymbol{e}_1$ and $\boldsymbol{e}_3$. Similar results for rods have also been reported by other authors; see for example Ni et al. [45] and the experimental work of Sabban et al. [46] for fibres with $L \approx 2\eta$. Byron et al. [44] found that rods mainly spin around their own symmetry axis at a rate that is half of the vorticity, while discs tend to tumble more than they spin. However, despite this difference, they found that the variance of the total rotation rate does not change with the particle shape, meaning that the total energy the particle subtracts from the flow to rotate remains the same.

The tumbling rotation rate of fibre-like objects has been extensively investigated [17–19]. Parsa and Voth [17] specifically investigate the tumbling rotation rate of rods with lengths within the inertial range of turbulence. They consider fibres with diameter d smaller than or equal to the Kolmogorov scale, and length L in the $2.8 \leq L/\eta \leq 72.9$ range. By using dimensional arguments, they predicted a scaling law that has been confirmed by their experimental measurements. In particular, they assumed that long rods can only rotate and align due to the action of eddies with comparable size. Based on this hypothesis, they found that, for rods with length scale L, the mean square rotation rate due to tumbling ($\boldsymbol{\Omega}_t$) scales like τ_L^{-2}, where τ_L is the time scale of eddies of size L, being defined as $\tau_L = L/u_L = L/(L\epsilon)^{1/3}$ where u_L is the velocity at length L and ϵ is the mean energy dissipation rate. Therefore, their dimensional argument gives $\langle \Omega_{t,i}\Omega_{t,i} \rangle \sim L^{-4/3}$ for L in the inertial range. Interestingly, they found a pretty good agreement between their predicted scaling and the results obtained from their experiments (see the left panel in Fig. 3). Their results, for the first time, pave the way for using long rods to access the spatial structure of the flow in the inertial range of turbulence, as discussed later in Section 3.2. Later, Bordoloi and Variano [18] considered particles with cylindrical shape and experimentally investigated their rotation rate in homogeneous isotropic turbulence. They considered elongated particles with maximum size within the inertial range, i.e. with $16 \leq L/\eta \leq 67$. However, unlike the previous work by Parsa and Voth [17], they considered particles with radial dimension larger than the Kolmogorov scale, i.e. $16 \leq d/\eta \leq 66$. Based on similar dimensional arguments as Parsa and Voth [17], they proposed a scaling law for the mean square total rotation (spinning + tumbling) rate $\boldsymbol{\Omega} = \boldsymbol{\Omega}_t + \boldsymbol{\Omega}_s$. They observed that in their space of parameters the scaling law is not based on L, but on d_{eq}, where d_{eq} is the diameter of the volume equivalent sphere, i.e. $\langle \Omega_i \Omega_i \rangle \tau_\eta^2 \sim \left(d_{eq}/\eta\right)^{-4/3}$; see the right panel of Fig. 3. According to their discussion, the difference with the previous scaling is due to the fact that for fibres with $d \ll \eta$, the radial dimension does not influence the rotation rate of the particle, while for $d \gg \eta$ it does, as it responds to the turbulent structures of the flow. The fact that this scaling law depends on d_{eq} and not on L or d, suggests that the rotation rate of anisotropic particles with size within the inertial range does not depend on their shape, confirming the results by Byron et al. [44] for sub-Kolmogorov particles. Later, Bounoua et al. [19] addressed the results of Parsa and Voth [17] and Bordoloi and Variano [18], and investigated the discrepancies of their proposed scaling laws. They experimentally studied the role of the aspect ratio of the fibres on their rotation rate, and found that the fibre inertia is at the origin of the discrepancy. They considered cylindrical rigid fibres and varied the length within the inertial range, considering aspect ratios λ in the $2.5 \leq \lambda \leq 80$ range. They found that the variance of the fibres tumbling rate follows $\langle \Omega_t \Omega_t \rangle \sim 1/(1+St_t^2)\tau_\eta^2 (\eta/L)^{4/3}$, where St_t is the tumbling Stokes number and $\tau_\eta = \sqrt{\nu/\epsilon}$ is the Kolmogorov time scale. When $St_t \ll 1$ the slender

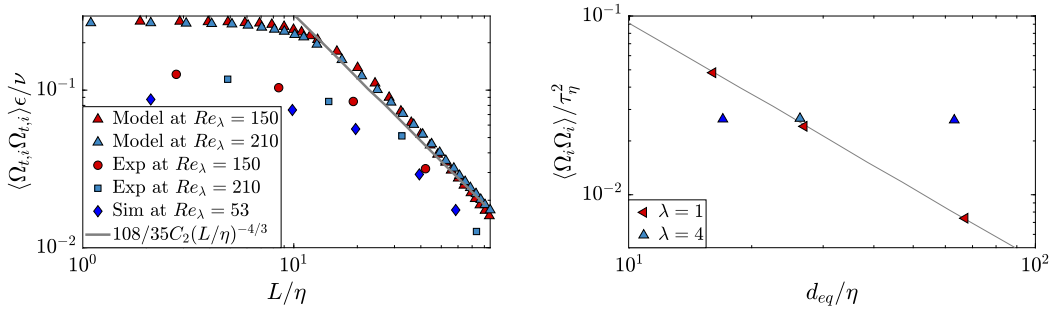

Fig. 3. Mean square rotation rate of long rods as a function of the rod length. Left: case with $d \ll \eta$ with data taken from [17]. Right: case with $d \gg \eta$, with data taken from [18]. d is the diameter of the particle, L is the length, while d_{eq} is the diameter of the volume equivalent sphere. In the right panel the blue triangles are for $\lambda = 4$, but replotted with respect to the cylinder's length and width instead of its volume-equivalent spherical diameter.

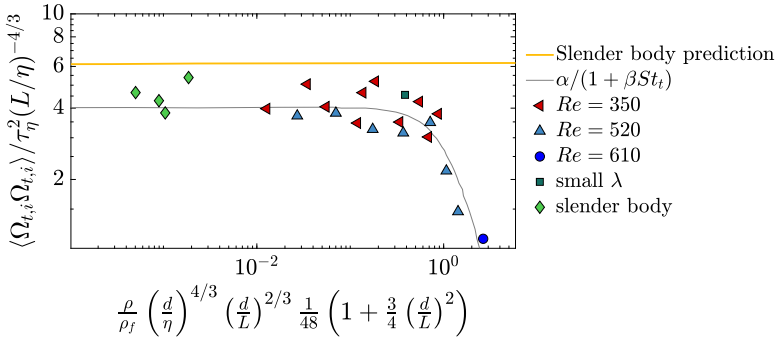

Fig. 4. Dependence of the tumbling rate of cylindrical solid fibres on the tumbling Stokes number St_t. Data taken from [19]. The green diamonds are the results from [17], while the blue square is from [18].

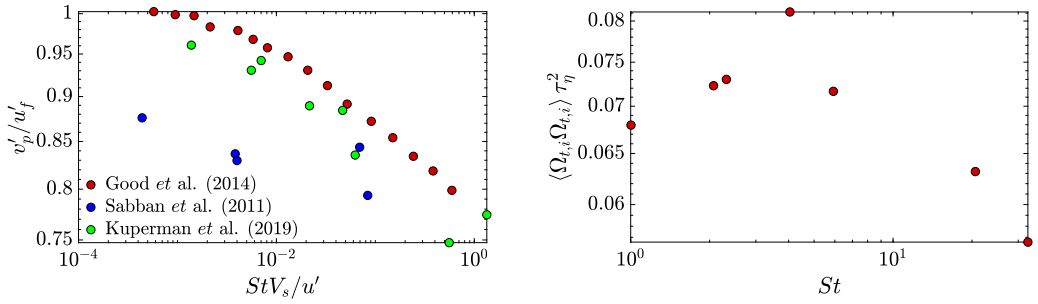

Fig. 5. Left: Root-mean-square ratios of fluctuating fibre (v_p') and fluid (v_f') velocities as a function of the fibre Stokes number. V_s is the still air settling velocity defined as $V_s = \rho_D^2\ g\left(\log(2\beta) + 0.193\right)/(16\mu)$ [see [36]]. The red circles are data from Good et al. [47]; the blue circles are data from Sabban and van Hout [48]; the green circles are data from Kuperman et al. [36]. Right: Normalised variance of the tumbling rate as a function of the Stokes number. For additional details on the experimental points we refer the reader to figures 5 and 13 of Kuperman et al. [36]. (For interpretation of the references to colour in this figure legend, the reader is referred to the web version of this article.) *Source:* Figures adapted from [36].

body theory is retrieved and $\langle \Omega_t\Omega_t\rangle \sim (L/\eta)^{4/3}$. When $St_t \gg 1$, instead, the variance of the tumbling rate is smaller as the forcing evolves on a much smaller time scale than the response time of the fibre. By using this scaling law they observed that both their measurements and those from Parsa and Voth [17] and Bordoloi and Variano [18] collapse pretty well; see Fig. 4.

The dynamics of rigid, heavy fibres change with their inertia. Kuperman et al. [36] experimentally detailed the effects of the inertia on the fibre dynamics in isotropic turbulence. They considered fibres with a Stokes number between $1 \le St \le 32.5$ and length larger than the Kolmogorov scale in the $3.6 \le L/\eta \le 17.3$ range. They observed that when increasing the inertia, the response of the fibres to the fluctuating fluid velocities decreases (see Fig. 5). This leads to a modification of the probability density functions of the fibre centroid velocity, which becomes narrower as the inertia increases. Regarding the tumbling rate, instead, they found that it does not decrease monotonically with increasing St, but found a peak at $St \approx 4$ (see Fig. 5). This is due to the fact that the total fibre rotation is comprised of both the spinning and tumbling. The ratio of spinning and tumbling rate depends also on the ability of the fibres to align with the vorticity vector. For small St, the fibre quickly aligns with the vorticity, and therefore its tumbling rate is rather small. When St increases, instead, the fibre is less able to align with the vorticity, and therefore the tumbling rate increases. For large St, however, the tumbling rate decreases again as fibres with large St, even if they do not align much with the vorticity field, respond slowly to the fluctuating field.

The alignment of rigid fibres with specific flow quantities has been investigated by Aswathy and Rosti [49], in the context of finite-size fibres suspended in a viscoelastic triperiodic turbulent flow. Their study is based on direct numerical simulations coupled with an immersed boundary method to deal with the fluid–solid interaction. They considered fibres with L in the inertial range of scales and $L \gg d$, and varied the Deborah number $De = \tau_p/\tau_f$ (it is a measure of the polymeric elasticity, with τ_p being the polymeric relaxation time and

τ_f the turnover time of the largest eddies of the flow) in the $0.3 \leq De \leq 7$ range; the Reynolds number is fixed at a value of $Re_\lambda \approx 310$. Like for fibres moving in a Newtonian flow, the authors found that they preferentially align with the intermediate eigenvector of the strain rate. For denser-than-the-fluid fibres they observed that the fibres are anti-aligned with the most and least extensional directions.

2.1.2. Turbulent channel flow

We now move to the behaviour of rigid fibres in turbulent channel flows. Several studies have investigated the dynamics of rigid anisotropic particles/fibres moving in a turbulent wall bounded flow. For example, we refer the reader to [10,50–57] for numerical simulations of a turbulent channel flow, to [58,59] for experiments of a turbulent channel flow laden with fibres, to [60] for experiments of a fibre laden turbulent pipe flow, to [61,62] for experiments of dilute fibre suspension in a turbulent channel with a backward-facing step, and to [63] for experiments of discs and fibres in a turbulent boundary layer.

Marchioli et al. [10] investigated the dispersion of rigid, highly elongated fibres in a turbulent channel flow at a friction Reynolds number of $Re_\tau = u_\tau h/\nu = 150$; here h is the channel half height and $u_\tau = \sqrt{\tau_w/\rho}$ is the friction velocity expressed in terms of the average wall shear stress τ_w and the density ρ. In their work, fibres are treated as prolate ellipsoidal particles with aspect ratio $1 \leq \lambda \leq 50$; here $\lambda = L/d$, with L and d being the semimajor and semiminor axes. According to their model, the fibre size is always assumed to be smaller than the Kolmogorov length-scale. The maximum length of the fibres is varied between $0.7 \leq L^+ \leq 36$, where the $\cdot^+$ superscript denotes quantities made dimensionless with u_τ and ν. The density of the fibres ρ_p, instead, has been varied between $10 \leq \rho_p/\rho_f \leq 10^3$; ρ_f is the fluid density. No back-reaction of the fibres on the flow has been considered. As shown in figure 1 of their paper, Marchioli et al. [10] found that close to the channel centre the fibres are randomly oriented, as the velocity gradients are rather weak. Close to the wall, instead, the velocity gradients are strong, and the fibres mainly align with the wall. Marchioli et al. [10] analysed the mean direction cosines of the fibres for different values of the inertia and of the aspect ratio, to investigate the fibre orientation statistics. They found that the alignment with the streamwise direction becomes stronger for longer fibres, but weaker for particles with larger inertia. They observed that the fibres are aligned with the mean flow at most 50% of the time, in agreement with the previous works by Zhang et al. [50] and Mortensen et al. [64]. They argued that the near-wall alignment imposed by the streamwise fluctuations, though statistically probable, is unstable and is not maintained for long times. They also observed that the fibre alignment with the spanwise direction decreases with their inertia [64], as spanwise velocity fluctuations are rather weak. Overall, they observed that longer fibres are more frequently aligned with the wall, suggesting a preferred seesaw-like rotation characterised by an alternate rotation of the fibre tips as the fibres are advected downstream (see their paper for further details).

Similar results have been found by Do-Quang et al. [22], that considered rigid finite-size fibres (rods) in a turbulent channel flow at $Re_\tau = 180$. They varied the length of the fibres in the $3.2 \leq L^+ \leq 24$ range, and considered two different fibre-to-fluid density ratios, i.e. $\rho_p/\rho_f = 1$ and 1.2. Unlike Marchioli et al. [10], Do-Quang et al. [22] also modelled the back-reaction of the fibres on the flow. The authors found that fibres accumulate mainly near the wall, at a distance of the order of the fibre length. Also, they found that the case with larger inertia shows a stronger accumulation indicating that there is some turbophoresis effect [15]. By following one fibre, they showed that this near-wall concentration is because, most of the time, the fibres are trapped in the high-speed streaks of streamwise velocity that populate the near-wall region [65]. They observed that the fibres move at roughly constant speed and angular velocity during most of the time, but sometimes they abruptly change direction of motion and rotation. In fact, in high-speed streaks the flow moves downwards and pushes the fibres towards the wall. Once the fibres interact with the viscous sublayer, or collide with the wall, they face a large torque and are thus pushed upwards. However, the upward motion is balanced by the downward motion of the fluid in the high-speed streaks, and the fibres remain trapped in the high-speed streaks until they reach an ejection-like region of the flow.

The dynamics of fibres changes with their Stokes number and with their length. Shaik et al. [58] and Shaik and van Hout [59] experimentally investigated the dynamics of straight rigid fibres freely moving in a fully developed turbulent channel flow at a friction Reynolds number of $Re_\tau \approx 435$. They varied the Stokes number and the length of the fibres in the $0.02 \leq St^+ \leq 0.34$ and $16 \leq L^+ \leq 66.8$ portion of the parameter space, and found that the wall-normal distribution of the fibres and their dynamics changes with St and L. Very close to the wall they found that the fibre concentration is low; a depletion layer arises in the immediate vicinity of the wall, with a width that decreases as St increases. In the buffer layer, $14 \leq y^+ \leq 24$, they found that except for the largest L, the fibres' velocity exceeds the mean fluid velocity as they preferentially accumulate in high speed regions [22]. Beyond the buffer layer, instead, they observed that the fibres lag the fluid. They report that the lag increases with L due to the increased drag. Their experiments also showed that L influences the intermittency of their velocity signal. In fact, longer fibres exhibit an increase probability of extreme transverse and wall-normal velocities, as they interact more effectively with larger and more energetic flow structures. Similarly, they observed that L influences the tumbling rate, with longer fibres tumbling at a higher rate that shorter ones. When looking close to the wall, they observed that irrespective of their length fibres preferentially align with the streamwise direction in agreement with the results of [10], leading to a substantial lack of fibre–wall interactions.

Several works investigated how the dynamics of anisotropic rigid particles in turbulent channels is influenced by their shape. Zhao et al. [55] observed that the statistics of the particles rotation, their concentration and their preferential sampling vary with the shape of the particles and do not depend only on their inertia. Indeed, a different shape modifies the preferential alignment of the particles, and therefore the way they respond to the fluid velocity fluctuations. For example, as a result of the different alignment, they found that at the channel centre oblated particles tend to rotate orthogonally to their symmetry axis, while prolate particles rotate around their symmetry axis. Baker and Coletti [63] experimentally addressed the influence of the asymmetric shape of rigid particles on their dynamics, investigating the behaviour of negatively buoyant discs and fibres in a turbulent boundary layer at a friction Reynolds number of $Re_\tau \approx 620$. For both discs and fibres they fixed the major axis length at a value of $L^+ \approx 50$, leading to a friction Stokes number of $St^+ = \mathcal{O}(10)$ for both cases. They found that irrespective of the shape, non spherical particles oversample high-speed fluid regions close to the wall [22]: despite their significant inertia, non spherical particles exceed the mean fluid velocity in the vicinity of the wall. They found that the shape of the particles influences their preferential alignment, modifying thus their response to the fluid velocity fluctuations. Fibres tend to align mostly in the streamwise direction, while discs mostly align their symmetry axis with the wall-normal direction, with what they referred to as a nose-up configuration. They observed that the this alignment is more stable for fibres than for discs; the former undergo strong tumbling near the wall, while the latter wobble around their wall-normal preferential direction. As a result of their different alignment, although having the same relaxation time, they observed that fibres and discs respond differently to the turbulent fluctuations, with the latter being slower. Based on this, they argued that for anisotropic particles the actual response time does not depend on the Stokes number only, but also on the preferential alignment of the particles and, therefore, on their shape.

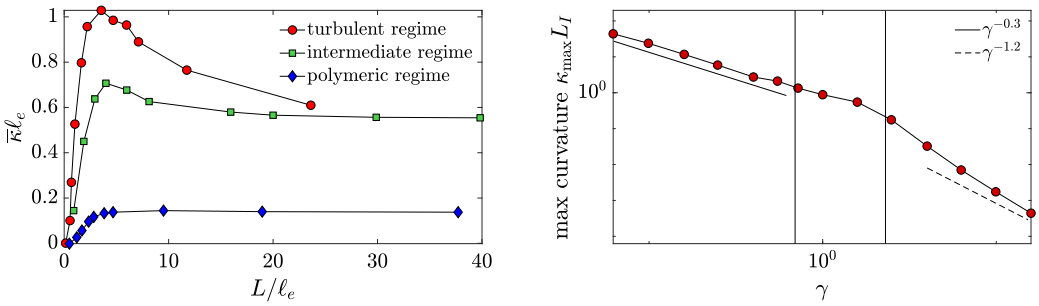

Fig. 6. Behaviour of the bending deformation of finite-size flexible fibres in a turbulent flow. Left: Evolution of the mean curvature $\overline{\kappa}$ as a function of the fibre length. Blue line refers to the polymeric regime, red line to the turbulent regime and green line to the intermediate one. Right: evolution of the maximum mean curvature $\overline{\kappa}_{\max}$ normalised with $\mathcal{L}$ as a function of the fibre stiffness γ. The turbulent regime is at the left side of the left vertical line, while the polymeric regime is at the right side of the right vertical line. (For interpretation of the references to colour in this figure legend, the reader is referred to the web version of this article.)
Source: Figure adapted from [68].

The dynamics of the fibres also depends on their symmetries. Alipour et al. [66] and Alipour et al. [67] experimentally investigated the influence of the curvature on the dynamics of long and rigid slender fibres ($L/D \gg 1$) freely moving in a turbulent channel flow. They fixed L and varied the friction Reynolds number of the channel between $180 \leq Re_\tau \leq 720$ to account for different fibre-to-fluid length scale ratios. Like for straight fibres, they observed that close to the wall non axisymmetric fibres preferentially sample high-speed regions, and that this tendency increases with the Reynolds number. They related this with their interaction with the coherent structures of wall turbulence; as Re increases, indeed, the sweep events close to the wall intensify leading to stronger wall-ward fluxes. Their results show that the curvature of the fibres influences the orientation of the near-wall fibres. For all cases rigid fibres tend to align with the major axis belonging to a plane parallel to the wall. Fibres with large curvature, however, tend to align their preferential axis with the streamwise direction. Fibres with low curvature, instead, are more sensitive to local flow conditions and are therefore less aligned with the streamwise flow direction.

2.2. Flexible objects

This section delves into the underexplored dynamics of flexible fibres in fluids, highlighting two key environments: homogeneous isotropic turbulence and turbulent channel flows. Initial studies, such as Gay et al. [68], categorise fibre behaviour by introducing length scales that differentiate between rigidity and flexibility, focusing on deformation without considering extensibility or torsion. Further, Dotto and Marchioli [69]'s work on turbulent channels reveals how fibre orientation and concentration are influenced by inertia and proximity to walls. These insights lay the groundwork for our investigation into flexible fibre motion in fluid flows.

2.2.1. Homogeneous isotropic turbulence

We start considering homogeneous isotropic turbulence. One of the first works to appear regarding flexible fibres is the one by Gay et al. [68]. They focused on the characterisation of the fibre deformation, that is the first step to understand their complex dynamics. To simplify the analysis, they start focusing on bending deformations only, neglecting the extensibility and the torsion of the fibres. When analysing the dynamics of flexible fibres in turbulent flows, three length scales can be introduced, i.e. the length of the fibre L, the elastic length ℓ_e which defines whether the fibre can be considered rigid ($L \leq \ell_e$) or flexible ($L \geq \ell_e$), and the integral scale of the turbulent flow $\mathcal{L}$. Based on these lengths, several regimes are possible. Considering only the case of flexible fibres ($L > \ell_e$) that are much longer that the dissipative Kolmogorov scale ($L \gg \eta$) three regimes are possible. In the first regime, the integral scale is much smaller than the elastic length ($L > \ell_e \gg \mathcal{L}$) and the fluid forcing on the fibre is uncorrelated at the scale of the fibre deformation. This regime is referred to as polymer regime. In the second regime, the fibre length lies in the inertial range ($\mathcal{L} \gg L > \ell_e$), and the forcing is correlated along the fibre. This case is called turbulent regime. Eventually, the third and intermediate regime ($L > \mathcal{L} > \ell_e$) is referred to the case for which the fibres experience a forcing correlated at small scales, but uncorrelated at larger scales. Gay et al. [68] studied the fibre deformation in the different regimes both experimentally and numerically. However, due to the prohibitive computational cost, they did not solve the full two-way coupling between the elastic fibre and the turbulent flow by direct numerical simulation (DNS), but used the so-called Kinematic Simulation Method [70], which is based on the use of random Fourier modes. They defined the mean value of the fibre curvature κ as

$$\overline{\kappa} = \frac{1}{L - 2\ell_e} \int_{\ell_e}^{L-\ell_e} \langle \kappa(s) \rangle \mathrm{d}s$$

to remove the effects from the fibre extremities where the curvature increases. When $L \leq \ell_e$ the mean curvature is taken as κ at $s = L/2$. They found that the dependence of $\overline{\kappa}$ on the fibre length L depends on the regime; see Fig. 6. In the polymer regime, the mean curvature increases with the fibre length, until it saturates to a value that does not depend on L. For the turbulent and intermediate regimes, instead, the mean curvature increases with L up to a maximum and then decreases for longer fibres. Therefore, due to the forcing correlation, long fibres are statistically less curved than shorter ones. They argued that this is due to a combined effect of viscous effects and inextensibility of the fibres (we refer the interested reader to their work for further details). Also, they investigated the dependence of the maximum mean curvature $\overline{\kappa}_{\max}$ as a function of the fibre rigidity γ, varying ℓ_e from the polymeric regime to the turbulent one. They found two different power laws (see Fig. 6), that well correlate with their dimensional analysis.

Besides the mean curvature, also the maximum curvature experienced by the fibres changes with L. This has been investigated in Olivieri et al. [27] by means of a massive DNS study where the fluid–solid interaction is dealt with an Immersed Boundary Method [71]. Here the authors considered both the case of iso-dense and denser-than-the-fluid fibres. Unlike Gay et al. [68], they did not introduce the elastic length scale, and based their discussion on a dimensional analysis of the dynamical equation of the fibres. In doing this, they found two different regimes depending on $\kappa_{\max}L$: for rigid fibres ($\kappa_{\max}L \gg 1$) the maximum curvature scales as γ^{-1}, while for sufficiently flexible ones the maximum curvature scales as $\gamma^{-1/3}$. They found that their data collapse pretty well with the theoretical scaling, with only small deviations for the denser-than-the-fluid fibres in the transition region between the two regimes; see Fig. 7.

In the same work, Olivieri et al. [27] characterised also the collective dynamics of flexible fibres, and considered the local concentration of the suspension to investigate the presence of clustering phenomena [see [15], for spherical particles], which is relevant for applications in several fields [1,8]. To measure the tendency of fibres to accumulate

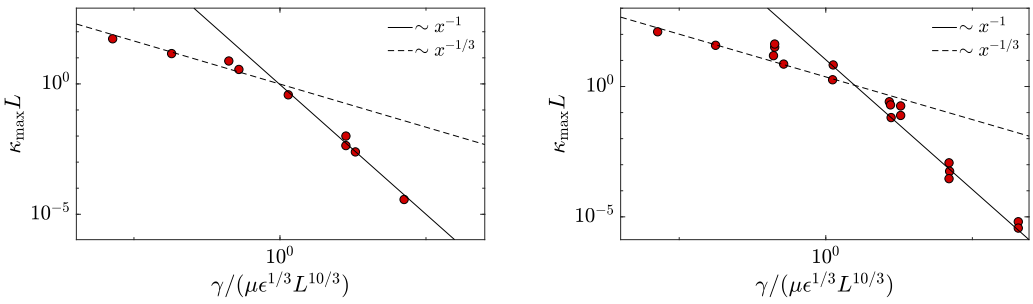

Fig. 7. Maximum fibre curvature as a function of the normalised bending stiffness for iso-dense fibres (left) and denser-than-the-fluid fibres (right). *Source:* Adapted from [27].

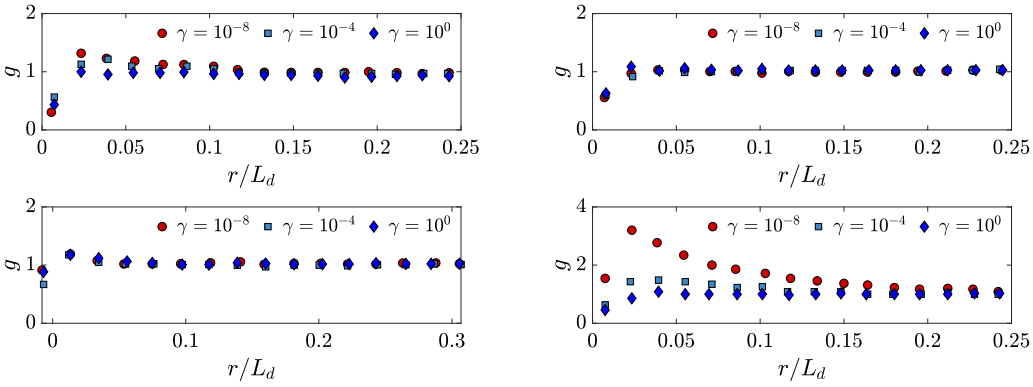

Fig. 8. Radial distribution function for iso-dense fibres (left) and denser-than-the-fluid fibres (right). Top is for short fibres, bottom is for long fibres. *Source:* Adapted from [27].

they used the radial distribution function RDF (or pair correlation), which indicates the probability of having a pair of particles at a given mutual distance. The RDF, thus, highlights the presence of accumulation at particular length scales. They found that for iso-dense fibres the clustering effect is essentially negligible for all the values of the fibre length and bending stiffness, highlighting the role of the inertia in the formation of clusters [72]. In contrast, for the denser-than-the-fluid fibres they found a richer phenomenology; see Fig. 8. First, they observed that the accumulation increases when decreasing the bending stiffness. According to the authors, this occurs as more flexible fibres adapt more easily to the local flow structure and therefore sample more frequently the regions of the flow with lower vorticity as point-particles do. Also, the highest peak in the RDF is found for long fibres. The authors argued that clustering is favoured in case of larger inertia and larger flexibility.

Some works have focused on the process of fibre fragmentation in turbulent flows. As an example, here we consider the work of Allende et al. [73]. They numerically investigate the fragmentation process of small inextensible inertialess fibres in homogeneous isotropic turbulence. They considered very thin fibres that can be approximated as inextensible Euler–Bernoulli beams immersed in a viscous fluid, with a negligible inertia. The backreaction of the fibres on the fluid is neglected. They considered $L \ll \eta$; this allows them to simulate the motion of the fibres by simply evolving in time the position of their centre of mass which is treated as a tracer. They then recover the fluid velocity along the fibre (and the resulting force) by assuming that the distribution is linear and exploiting the fluid velocity derivative tensor. They focus on tensile and flexural failures, i.e. failures that occur because the internal tension is higher than a given threshold and because the curvature of the fibre exceeds a certain threshold. They found that for both cases the break up occurs when the fibre runs into a flow region with large strain where it is either stretched above the internal cohesive forces or compressed such that it buckles and fractures under the excessive bending. In their analysis, they observe that the tensile failure always occurs when the fibre is stretched by the flow, and has a straight configuration. In this case, the tension is maximum at its centre and the break up produces two fragments of equal size. For flexural failure, instead, they observed a more intricate scenario. In this case the fragmentation occurs when fibres develop a buckling instability and the size of the fragments depends on the properties of the most unstable buckling mode. By using their simulations they found that the fibres' fragmentation rates can be expressed by means of the turbulent stretching rates and proposed empirical fitting laws.

2.2.2. Turbulent channel flow

We now move to the behaviour of flexible fibres in turbulent channels. Few studies have addressed the motion of fibres in turbulent channels, among whose we cite the work by Dotto and Marchioli [69].

Dotto and Marchioli [69] investigated the behaviour of flexible fibres longer than the Kolmogorov length scale in a turbulent channel at $Re_\tau = 150$, with a focus on their translational and rotational behaviour. In their numerical work the fibres are modelled as chains of sub-Kolmogorov rods, connected though ball-and-socket joints, that enable bending and twisting under the action of the local fluid velocity gradients. They observed that the orientation of the fibres changes with the fibre inertia and with the distance from the wall (see Fig. 9). They investigated the probability density function of the fibre mean orientation in the streamwise (x) and wall-normal (z) directions, i.e. $\langle o_x|_G \rangle$ and $\langle o_z|_G \rangle$. When $o_j = 1$ the fibre is aligned with the j_{th} flow direction, while $o_j = 0$ means that the fibre is orthogonal to such direction. Since the fibres are flexible, they computed the orientation of each fibre averaging along each sub-Kolmogorov element. For small inertia ($St = 1$), the near-wall PDF is negatively skewed for $\langle o_x|_G \rangle$ and positively skewed for $\langle o_z|_G \rangle$. In this case, thus, fibres are preferentially aligned with the streamwise flow direction and perpendicular to the mean shear. Interestingly, this trend is more evident when longer fibres are considered. In the bulk flow the PDF are more symmetric and more insensitive to the fibres length. In fact, in the bulk region the flow is more

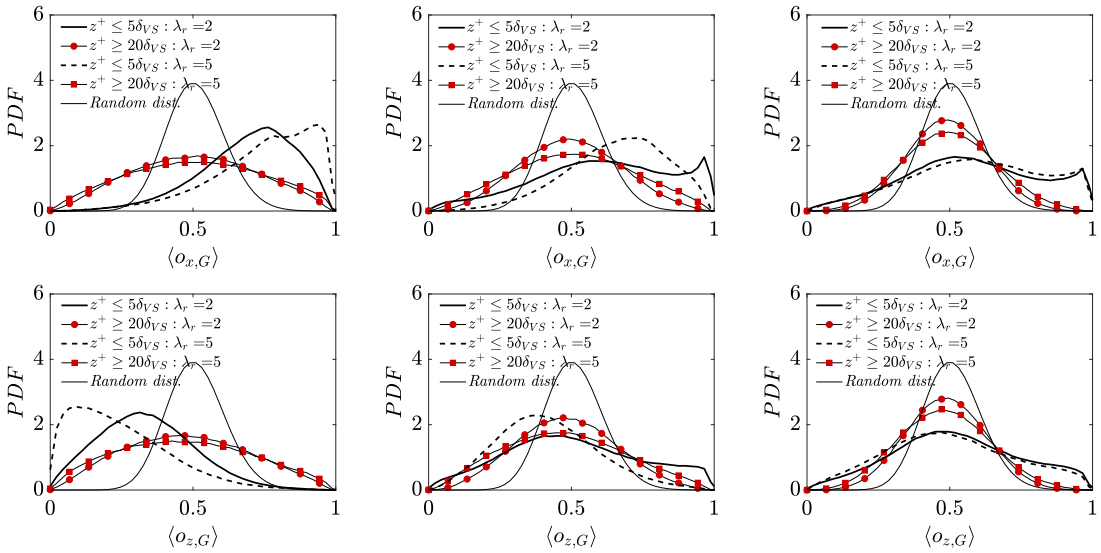

Fig. 9. Fibre mean orientation in the streamwise (top) and wall normal (bottom) directions. From left to right $St_r = 1$, $St_r = 5$ and $St_r = 30$. The thin solid line corresponds to the PDF of a random distribution of orientation in a three-dimensional domain.
Source: Adapted from [69].

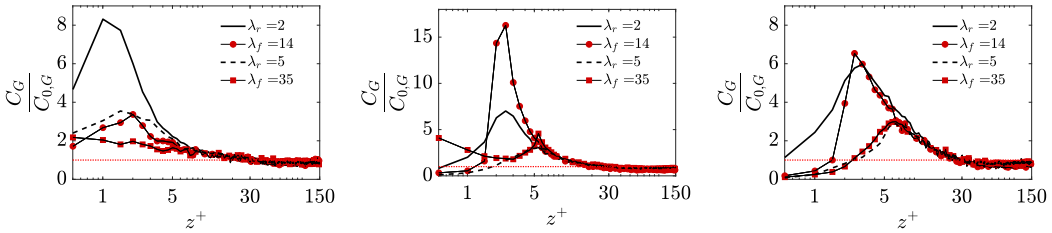

Fig. 10. Instantaneous fibre concentration along the wall-normal direction. From left to right: $St_r = 1$, $St_r = 5$ and $St_r = 30$. C_G is the number density defined as $C_G(t) = N_{f,s}(t)/V_s$, where $N_{f,s}(t)$ is the number of fibres with centre of mass G falling in the considered fluid slab at time t, and V_s is the volume of the fluid slab. $C_{0,G}$ is the concentration at initial time. The figure refers to $t^+ = 1250$ and is obtained with a number of slabs of $N_s = 150$.
Source: Adapted from [69].

homogeneous and isotropic, leading to a weaker preferential alignment. When increasing the Stokes number the symmetry in the bulk region is maintained, while the behaviour of the near-wall PDF changes. For intermediate St the PDF are only slightly skewed, indicating that the tendency for a preferential alignment decreases. For large St the PDF recover an almost symmetric distribution as in this case fibres are less influenced by the fluid motion. Note that for long fibres, the authors found a sharp peak in the probability density function (PDF) of $\langle o_x|_G \rangle$ at values close to unity, which is accompanied by a larger drop in the PDF of $\langle o_z|_G \rangle$. This is due to the fibre trapping in a thin region close to the wall, where the geometric constraint imposed by the wall imposes the streamwise alignment of the fibres.

Dotto and Marchioli [69] investigated also the influence of the fibre flexibility on their concentration. They observed that the concentration of flexible fibres in the near-wall region is always higher than that of rigid fibres, indicating that flexible fibres face a stronger wallward turbophoretic drift; see Fig. 10.

3. What can we do with fibre-like objects?

The second part of the paper explores the interaction of fibre-like objects with fluid flows, emphasising their behaviour in turbulent flows and applications ranging from drag reduction to innovative flow measurement techniques. Initial sections discuss the potential of rigid and flexible fibres to modify flow characteristics and reduce turbulent drag, observed through various experimental and numerical studies. Later, the paper introduces fibre tracking velocimetry (FTV), a novel method for capturing detailed properties of turbulent flows, comparing its effectiveness to traditional particle-based measurement techniques. The discussion underscores the versatility of fibres as both flow modifiers and measurement tools, highlighting their significance in advancing our understanding of fluid dynamics.

3.1. Fibre-like objects for drag reduction

Over the last decades there has been a large number of studies dealing with the reduction in turbulent friction losses by the dilute addition of additives such as polymers [74,75], surfactants [76,77] and fibres [51,54,57,78]; we refer the interested reader to the recent review by Marchioli and Campolo [79]. The reduction of turbulent drag by the addition of fibre-like objects has been first observed experimentally in suspension involving a wide array of material, for example paper, asbestos, and colloidal crystals [80,81]. Some of these material can effectively be considered as rigid rods to a good approximation. Compared to the flexible polymers [74], these types of additives have been less studied as they yield low drag reduction or require much larger concentrations to achieve the same amount of drag reduction as that obtained with flexible polymers additive. However, the use of fibrous additives is interesting as fibres are more resistant to shear degradation than flexible polymers. As such, the possible use of fibres for drag reduction purposes is very promising.

An interesting study of drag reduction induced by rigid neutrally-buoyant fibres was given by Paschkewitz et al. [51]. They considered rigid neutrally buoyant fibres with length much smaller than all the scales of the turbulent flow, and neglected all the inertial effects on the scale of the fibres. They modelled the fibres using the Jeffrey's

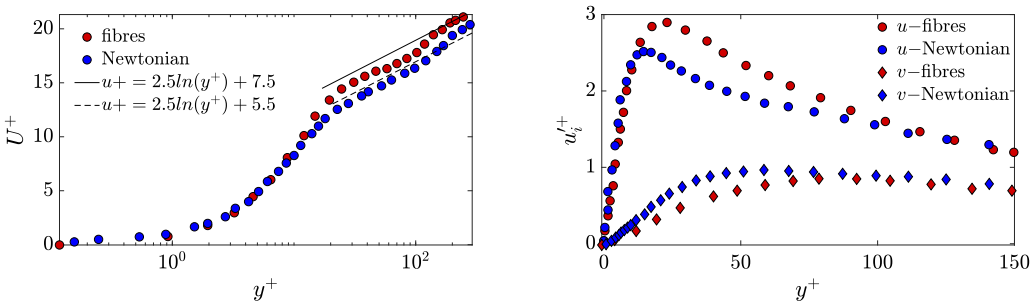

Fig. 11. Influence of small fibres on a turbulent channel flow. Left: Mean velocity profile. Right: r.m.s. of the velocity fluctuations. The + superscript denotes viscous units. Data taken from [51].

equation and the Fokker–Planck equation, and considered a turbulent channel flow. Their simulations reveal values of drag reduction up to 26%, with the maximum observed in semi-dilute condition. As shown in Fig. 11, they found that the effect of the fibres is qualitatively similar to what seen in polymeric simulations. Accordingly to other drag-reduced flows [82,83], the presence of the fibres leads to an upwards shift of the mean velocity profile in the logarithmic region, which is indicative of a thickening of the viscous sublayer. Notably, they found that the root mean square of the velocity fluctuations resemble what seen in polymeric simulations: the streamwise fluctuations increase and their peak moves upwards, while the intensity of the wall-normal and spanwise fluctuations decreases. By inspecting the near-wall region, they observed that the presence of the fibres weakens the near-wall vortex structures and increases their size. The spacing between the high- and low-speed streaks [84], instead, increases due to the presence of the particles, moving from 100 wall units to 150. Based on these results, they proposed a mechanism for the fibre-induced drag reduction, that includes the interaction of the fibres with the near-wall vortices. In plain words, fibres strongly align in the (y, z)-plane generating large normal and shear stresses. These stresses create a force opposite to the Newtonian acceleration in the spanwise and wall-normal directions that weaken the near-wall vortex structures and lead to drag reduction. Then fibres realign with the mean flow and the near-wall vortices reform, sustaining this weakened turbulence. Later, Paschkewitz et al. [52] experimentally confirmed the ability of small rigid rods to effectively reduce drag. They experimentally and numerically considered a zero pressure gradient turbulent boundary layer where small rigid rods with different concentration were injected. They found drag reduction up to 10%. The spatial development shows an initial drag reduction region followed by a region of quasi-steady-state drag reduction where the drag reduction fluctuates about a mean value as the fibres undergo the process of alignment, stress generation and relaxation as previously discussed. The increase of the fibre concentration does not increase the drag reduction, but shifts downstream the region where it is actually achieved.

Following these promising results, Moosaie and Manhart [54] developed a two-way coupling simulation technique for a dilute suspension of rigid fibres to study the turbulent drag reduction by rigid fibres in a turbulent channel flow at the nominal friction Reynolds number of $Re_\tau \approx 180$. They solve the Navier–Stokes equations with direct numerical simulations, and treated the suspended microstructure in a Lagrangian manner using a particle tracking scheme. On each Lagrangian path a cluster of sampling fibres is followed, and the conformation of each cluster is computed using a direct Monte Carlo method. Their results confirmed the previously reported features of a fibrous drag reduced channel flow. They indeed found a vertical shift of the logarithmic law region of the mean velocity profile and an increase of the spanwise spacing between the near-wall streaks.

In a more recent work, Di Giusto and Marchioli [57] found that it is possible to achieve drag reduction in a turbulent channel flow, also by using long fibres. Unlike the previous works, indeed, they considered a different portion of the space of parameters, i.e. much longer fibres with a length that extends up to the inertial range, and considerably smaller volume fractions, i.e. $\Phi_V \approx 10^{-4}$ and $\Phi_V \approx 10^{-5}$; $\Phi_V = V_p/(V_f + V_p)$ where V_f and V_p are the volumes occupied by the fluid and the particles respectively. Their simulations are based on an Eulerian Lagrange approach where fibres are modelled as chains of constrained sub Kolmogorov Rods. They obtained the two-way coupling using the Exact Regularised Point Particle Method [85]. In their analysis they considered a turbulent channel at a friction Reynolds number of $Re_\tau = 150$ varying the fibres' Stokes number in the $0.01 \leq St \leq 10$ range. They found that also in the portion of the space of parameters they have considered drag reduction is possible. They highlight the importance of the volume fraction which is the key parameter to determine the intensity of the drag reduction, and found that the mass load plays a role: a minimal amount of inertial fibres is needed for the onset of drag reduction, below which drag increases.

Considering more in general non spherical objects, it is worth mentioning that Ardekani et al. [23] showed that also oblate rigid particles are effective in reducing drag, in contrast to what observed for spherical particles [86–88]. They considered a suspension of finite-size oblate spheroidal particles with aspect ratio $\lambda = 1/3$ freely moving in a turbulent channel flow at a friction Reynolds number of $Re_\tau = 180$, and used an immersed boundary method to properly solve the fluid around each particle [89]. They found that the amount of drag reduction progressively increases with the volume fraction of the suspension, up to a value of $\approx 8\%$ for $\Phi_V = 0.15$ (see Fig. 12). In a particle laden turbulent channel flow, there are two important factors that determine the overall drag, i.e. the turbulence activity in the suspension and the particle-induced stresses, which are not only due to the increase of the suspension effective viscosity in presence of particles, but also due to their distribution along the channel. Picano et al. [86] have shown that, for suspension of spheres, a particle layer forms close to the wall, and this causes extremely large particle-induced stresses that are therefore responsible for the large increase of the total drag, although the turbulence activity reduces for high volume fractions. In case of oblate particles the scenario is different; see Fig. 13. In fact, a particle layer close to the wall does not form, meaning that the particle-induced stresses are rather weak. As the volume fraction increases, indeed, the relative momentum transfer due to the Reynolds stresses decreases, but the particle-induced stress does not increase enough to compensate it, leading thus to a global decrease of the drag.

3.2. Fibres as a measurement technique

Over the last years several contributions have shown that fibres with finite size can be effectively used as tools for measurements of the unperturbed flow. This research field considers both rigid and flexible fibres, and enables a reliable measure of two-points statistics of the flow. Notably, based on these argument a new experimental technique, named "fibre tracking velocimetry" has been introduced [35], which substantially improves the well-known techniques based on particle

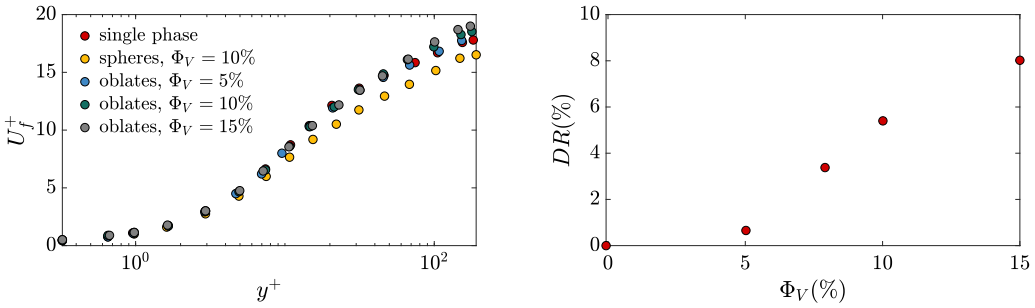

Fig. 12. Drag reduction by oblate rigid particles in a turbulent channel flow. Adapted from [23]. Left: Mean fluid velocity profiles for different volume fractions. Right: dependence of the amount of drag reduction DR on the volume fraction of the suspension Φ_V.

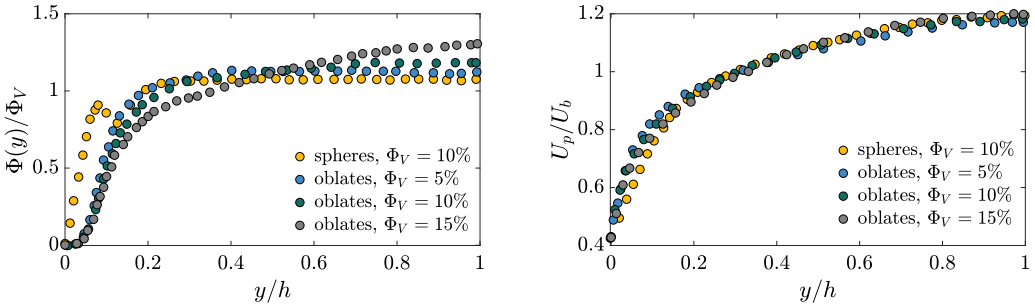

Fig. 13. Profiles of the solid-phase average mean local volume fraction $\Phi(y)$ (left) and of the mean particle velocity profiles $U_p(y)$ (right).
Source: Adapted from [23].

tracers as the particle image velocimetry (PIV) and the particle tracking velocimetry (PTV). In this section we report the main contributions and distinguish between rigid and flexible fibres.

3.2.1. Rigid fibres

Cavaiola et al. [25] were the first to address the possibility of measuring the whole structure of the flow velocity gradient by means of a Lagrangian tracking of assembly of rigid fibres. The idea is to replace single particles typically used in particle image or tracking velocimetry (PIV/PTV) to measure single-point fluid properties [90], with fibres in order to access two-points and multi-points fluid properties. In this proof of concept work, Cavaiola et al. [25] considered laminar flows and focused on cellular flows, which are considered as a conceptual representation of eddies of a turbulent flow. They considered the Arnold–Beltrami–Childress (ABC) flow [91], which is a periodic solution of the Euler's equations, with rigid fibres of length $L/L_d = (2\pi)^{-1}$; where L_d is the domain size. To assess the influence of the inertia of the fibres they varied the Stokes number between $0.01 \leq St \leq 4$, where $St = \tau_s/\tau_f$ with $\tau_f = L_d/U$ being the characteristic hydrodynamic time scale and τ_s the fibre Stokes time, i.e. the relaxation time of a fibre immersed in a viscous flow (it is a measure of the fibre inertia compared to the flow and quantifies the strength of the coupling between the two phases).

In this idealised framework, Cavaiola et al. [25] found that fibres cannot be effectively used to measure single point flow quantities, as done in PIV and PTV techniques with tracer particles. In fact, even at the smallest Stokes number they have considered, the velocity magnitude of the fibres' ends significantly differs compared with the velocity magnitude of the unperturbed flow. However, they found that, provided that the Stokes numbers is small enough, the velocity difference between the two end points of the fibres $\delta \boldsymbol{V} = \boldsymbol{V}_B - \boldsymbol{V}_A$ projected on a plane normal to the direction parallel to the fibre end to end distance $\hat{\boldsymbol{r}}$ (see Fig. 14), matches the unperturbed fluid velocity difference $\delta \boldsymbol{u} = \boldsymbol{u}_B - \boldsymbol{u}_A$ projected on the same plane, i.e.

$$\delta \boldsymbol{V} \cdot \hat{\boldsymbol{r}}_\perp = \delta \boldsymbol{u} \cdot \hat{\boldsymbol{r}}_\perp;$$

see figure 4 of their paper.

Note that with unperturbed fluid velocity we refer to the velocity of the fluid in absence of the fibre. The projection along the normal direction to the fibre is crucial for the fibre to be a proxy of the unperturbed flow velocity differences. If the velocity difference is projected along a generic direction the above agreement is not present, due to the fibre inextensibility that makes the velocity difference in the direction parallel to the fibre to be null. The projection to the normal direction, instead, washed out this constraint. Interestingly, provided that the fibre is small enough compared to the fluid scales, the projected end to end velocity difference is a measure of the velocity derivative at the fibre centre of mass. In view of this, the authors suggested that this may enable the access to the full fluid velocity gradient tensor $\partial u_i/\partial x_j$, by properly assembling N_f fibres. By considering the simple two-dimensional case, due to the incompressibility constrain the actual unknowns for the velocity gradient tensor are three. Therefore, the complete tensor can be evaluated using an assembly of $N_f = 3$ fibres (see the right panel of Fig. 14), and solving the following system:

$$\begin{cases} \delta V_\perp^{(1)} = \frac{\partial u_i}{\partial x_j} \hat{r}_j^{(1)} \hat{r}_{\perp,i}^{(1)} \\ \delta V_\perp^{(2)} = \frac{\partial u_i}{\partial x_j} \hat{r}_j^{(2)} \hat{r}_{\perp,i}^{(2)} \\ \delta V_\perp^{(3)} = \frac{\partial u_i}{\partial x_j} \hat{r}_j^{(3)} \hat{r}_{\perp,i}^{(3)}. \end{cases} \tag{1}$$

In view of the above discussion, the ability of elongated solid objects, like fibres, to move within the flow without significantly altering it is of large interest for the development of non intrusive measurement techniques. This point has been also addressed by Cavaiola and Mazzino [92], by investigating whether self-propelled objects (solid objects that may possess inertial and internal elastic degree of freedom) may detect some features of the unperturbed flow field, despite their disturbing presence. They observed that for a wide range of flow and swimmer Reynolds numbers, the swimmers are able to sense hydrodynamic signal with quite good accuracy. In fact, despite the perturbation due to the swimmer motion, there are some hydrodynamic observables that are practically unaffected by the swimmer motion. For

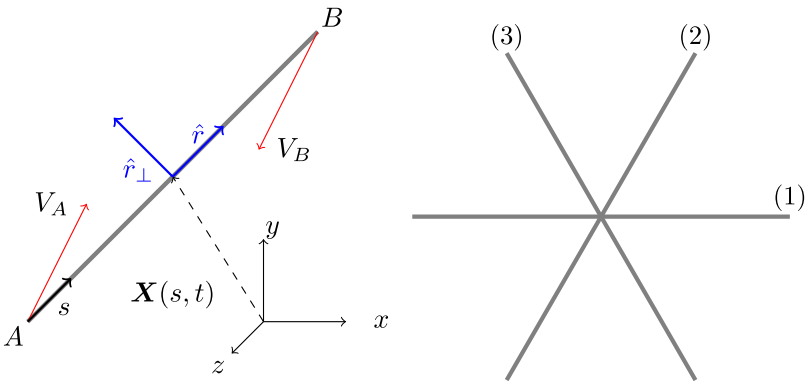

Fig. 14. Left: Sketch of a generic fibre and of the local reference system. $\hat{\boldsymbol{r}}$ refers to the direction parallel to the end to end distance, while $\hat{\boldsymbol{r}}_\perp$ refers to the normal to the fibre direction. Right: Assembly of $N_f = 3$ fibres that can be used in the two-dimensional case to evaluate the complete velocity gradient tensor.

example, they cite the velocity differences evaluated at the swimmer ends, projected along a direction on a plane normal to the swimmer orientation. In agreement with the results of [25], they observed that for short swimmers, this kinematic observable reduces to the flow derivative along that direction.

Following the work by Cavaiola et al. [25], Brizzolara et al. [35] proposed an experimental techniques named "fibre tracking velocimetry" (FTV), which aims at measuring two-points statistics of turbulent flows. It consists of spreading rigid fibres in the flow, and tracking their position and orientation in time. The authors claim that this method is superior to the traditional methods based on tracer particles, in particular when measuring the two-point statistics of turbulence. In fact, this method fits perfectly the necessity of measuring two-point statistics in the inertial range, in case where high particle concentration is hardly reachable or maintainable in time. The FTV technique is expected to be relevant when measuring quantities related to spatial velocity gradients, such as energy dissipation. In fact a well-known issue of tracer-based techniques is the evaluation of two-point statistical quantities, which are of special interest in turbulence. In a turbulent flow the relative distance between two particles that initially are close enough grows in time as $\sim t^{3/2}$, following the Richardson diffusion law [93]. This makes hard the use of particle tracers to obtain converged two-point statistics, as they tend to separate. A further situation where particle tracers are weak is when measuring quantities related to the velocity gradient tensor such as the energy dissipation rate. Indeed, the only way to access to these measures is by using an extremely high number of particles, that may alter the flow statistics. All these problems are overcome when using the FTV, as the measures are simply based on the fibre end to end velocity differences projected in to the normal to the fibres direction [25]. Note that the rigidity of the fibres in this technique is essential, as it ensures that the distance between the two ends is constant. By virtue of this constrain, indeed, it is possible to investigate the behaviour of eddies of a selected size. Note that in the FTV method, to be a proxy of turbulent eddies, the fibres must fulfil two simple conditions: (i) the length of the fibre has to be comparable to the size of the eddy under consideration; (ii) the inertia of the fibre has to be negligible or, in other words, the Stokes number has to be low [25,92].

Besides, exploring the feasibility of the FTV technique by means of numerical simulations, Brizzolara et al. [35] performed a laboratory experiment within a water tank and validated it, by means of a comparison with the PTV technique. They used a set up where both the PTV and FTV perform well. Fig. 15 shows the reliability of the FTV measurements showing a good agreement between the PTV and FTV measurements of the transversal structure functions and of the turbulence dissipation rate.

Besides the use of rigid straight fibres for measuring fluid phase properties, several authors have considered particles with complex and different shapes suggesting that, after calibration, following their motion may provide a powerful new way to analyse the dynamics of turbulent flows. Among the others, we cite the particles introduced by Kramel et al. [94]. These particles are called chiral dipoles, because of their similarity to electrical dipoles (see figure 1 of their paper). When placed in a pure strain flow, due to the high aspect ratio, the chiral dipoles tumble and align with the extensional strain direction $\hat{\boldsymbol{d}}$. Then, due to the presence of the helices, the chiral dipole couples with the strain flow, and produces a solid body rotation $\boldsymbol{\Omega} = \Omega_d \hat{\boldsymbol{d}}$, where Ω_d is the spinning rate. In their paper, Kramel et al. [94] characterised the response of the chiral dipole to a pure strain flow, and showed that the mean spinning rate depends on both the aspect ratio and the pitch of the particle; the pitch of the dipole is defined as the length along the particle for a complete turn of the helices, divided by their diameter. By using this type of particles and measuring their rotations, the authors claim that it is possible to analyse the dynamics of turbulent flow, measuring for example stretching experienced by orientable elements in turbulent flows [95].

3.2.2. Flexible fibres

The use of flexible fibres to measure two-point, and more generally multipoint, statistics of turbulence require the understanding of the dynamics of a flexible fibre freely moving in a three-dimensional fully developed turbulent flow. With this in mind, Rosti et al. [32] investigated the dynamics of a flexible fibre moving in homogeneous isotropic turbulence (HIT), and presented a phenomenological theory to describe the interaction between the fibre elasticity and the turbulent flow, extending the previous works by Brouzet et al. [96] and Verhille and Bartoli [97] to the inertial range of scales. Their theory is based on simple arguments. They observed that two characteristic timescales can be identified for the fibre: (i) the viscous time scale $\tau_\mu = 2\rho_1/\mu$ obtained by balancing the fibre inertia with the viscous damping, and (ii) the fibre elastic time $\tau_\gamma = \alpha(\rho_1 L^4/\gamma)^{1/2}$ obtained by balancing the fibre inertia with the bending rigidity; ρ_1 denotes the linear density of the fibres. They argue, therefore, that depending on the value of the damping ratio $\zeta = \tau_\mu/\tau_\gamma$ different regimes are expected. In the underdamped regime ($0 \leq \zeta \leq 1$) the elasticity is expected to strongly affect the fibre dynamics, while in the overdamped regime $\zeta > 1$ the elastic effects are expected to be strongly inhibited. Here we are interested on the underdamped regime. As shown in Fig. 16, for large elasticity (small γ) the fibre is deformed only by large values of the strain, and rapidly reacts oscillating at its characteristic frequency to restore the straight position. For small fibre elasticity (large γ), instead, the fibre does not resit the deformation and it is slaved to the turbulent fluctuations. The bending rigidity separating these two behaviours γ_{crit} can be extracted from a resonance condition between the fibre elastic time τ_γ and the eddy turnover time $\tau_f(r) = r^{2/3}\epsilon^{-1/3}$ evaluated at the fibre scale L [32]. In view of this, the scenario is the following: when

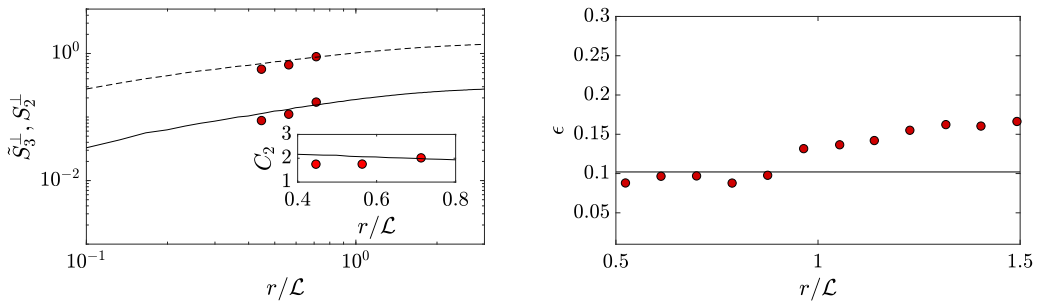

Fig. 15. Comparison between PTV and FTV in the experiments by [35]. Left: Second- and third-order transverse velocity structure functions ($S_2^{\perp}$ and $S_3^{\perp}$) from experiments. Solid and dashed lines are for PTV, while symbols denote statistics obtained with FTV. Right: Comparison between the turbulence dissipation rate evaluated with FTV and PTV. The solid line refers to the FTV measures, while the red circles to the PTV measurements.
Source: Adapted from [35].

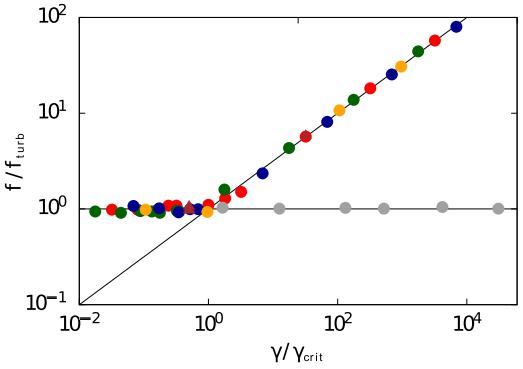

Fig. 16. Fibre oscillation frequency as a function of the fibre bending rigidity. Blue: $L/L_d = 0.12$ and $\rho_1/(\rho_f L_d^2) = 0.042$. Red: $L/L_d = 0.16$ and $\rho_1/(\rho_f L_d^2) = 0.042$. Green: $L/L_d = 0.20$ and $\rho_1/(\rho_f L_d^2) = 0.042$. Orange: $L/L_d = 0.16$ and $\rho_1/(\rho_f L_d^2) = 0.014$ or 0.125. Grey: $L/L_d = 0.16$ and $\rho_1/(\rho_f L_d^2) = 0$. Brown triangles: $L/L_d = 0.16$ and $\rho_1/(\rho_f L_d^2) = 0.042$, passive scalar cases. ρ_1 is the fibres linear density, ρ_f is the fluid density and L_d is the size of the domain. (For interpretation of the references to colour in this figure legend, the reader is referred to the web version of this article.)
Source: Adapted from [34].

$\gamma < \gamma_{crit}$ the fibre oscillates accordingly with the turbulence frequency $1/\tau_f(L)$, while for $\gamma > \gamma_{crit}$ the fibre oscillates following the first fibre normal mode with frequency $1/\tau_\gamma$.

The key result of Rosti et al. [32], later expanded in Rosti et al. [34], is that when $\gamma/\gamma_{crit} < 1$ and the fibre is locked to the frequency of the turbulent eddies of the same size, it is a good proxy of the velocity fluctuations at the same scale. In view of this, Rosti et al. [32] proposed for the first time to use flexible fibres to reveal the turbulent features at different scales. This is clearly visible in Fig. 17, where a comparison between the statistics based on the fibre flapping and on the Eulerian measurements are compared. This clearly states that the flow can be seeded with several elastic objects, potentially of different lengths in order to measure eddies of different size [34]. However, it should be noted that an increase of the concentration of the dispersed phase may modify the flow and increase the importance of the fibre-flow feedback [27], rendering the process of utilising fibres to gather flow statistics in vain. In this case the theory should be modified to account for the fluid phase modulation.

Similarly to the above discussed FTV based on rigid fibres, Hejazi et al. [33] proposed flexible particles of a different shape to properly extract the flow velocity gradient. They considered particles made of several slender arms, and showed that by tracking its rotation and the deformation of the arms one can measure the flow velocity gradient. In a generic three-dimensional incompressible flow there are eight free parameters in the velocity gradient tensor. If the particle is sufficiently isotropic, it rotates with the fluid vorticity. Therefore, the measure of the solid body rotation allows to reconstruct the three components of the velocity gradient tensor. The remaining five parameters can be extracted from the deformation of the n particle arms. The orientation of each arm requires the measurement of in-plane and out-of plane angles, providing a total of $2n$ measurements. Since three Euler angles are needed to specify the orientation of an undeformed particle in space, the total number n of arms needed to determine the five remaining parameters is such that $2n - 3 \geq 5$. This means that for properly measuring the complete flow velocity gradient in a three-dimensional flow, we need to compute the deformation from their equilibrium of at least $n = 4$ arms. In their proof of concept experimental study, Hejazi et al. [33] considered a two-dimensional shear flow and measured the complete velocity gradient tensor by means of a 3D printed deformable triad, i.e. a particle with $n = 3$ arms separated equally by $2\pi/3$ radiants. They found that the value of the magnitude of the strain deduced from the instantaneous particle deformation oscillates around an average value that matches the actual strain. Clearly, this type of particles can provide a measurement of the instantaneous strain rate tensor in the flow as long as the particle deformation relaxation time is shorter than the time scale associated with the velocity gradients.

4. Conclusions and future developments

This comprehensive review has examined the dynamic interplay between turbulent flows and fibre-like objects, with a main focus on anisotropic particles larger than the Kolmogorov scale. The insights provided here extend beyond the previously dominant studies on smaller fibres, offering new perspectives on the behaviour of both rigid and flexible fibres within turbulent flows. The review has highlighted the complex interactions of these fibres with flow properties, their organisation in various flow types, and their potential applications in engineering and environmental contexts.

The behaviour of fibre-like objects in turbulent flows, whether rigid or flexible, introduces significant complexities due to their anisotropic character. Their motion, characterised by tumbling, spinning, and preferential alignment with flow properties such as vorticity or strain rate, impacts both the fluid and the solid phases. These interactions become even more intricate when considering fibres that are flexible and subject to deformation, exhibiting complex motion influenced by various flow properties.

From a numerical perspective, advancements in computational power and techniques like immersed boundary methods have substantially enhanced our understanding of these interactions. Additionally, the review has underscored the importance of considering two-way coupling in scenarios with significant fibre concentrations or flexibility.

One of the significant applications of these studies lies in the use of fibre-like objects for turbulent flow measurements. Techniques like Fibre Tracking Velocimetry have been introduced, offering new methods to measure properties of turbulence at fixed length scales.

Looking ahead, there are several areas where further research could be highly beneficial. Firstly, expanding our understanding of the interactions between flexible fibres and turbulent flows will be crucial,

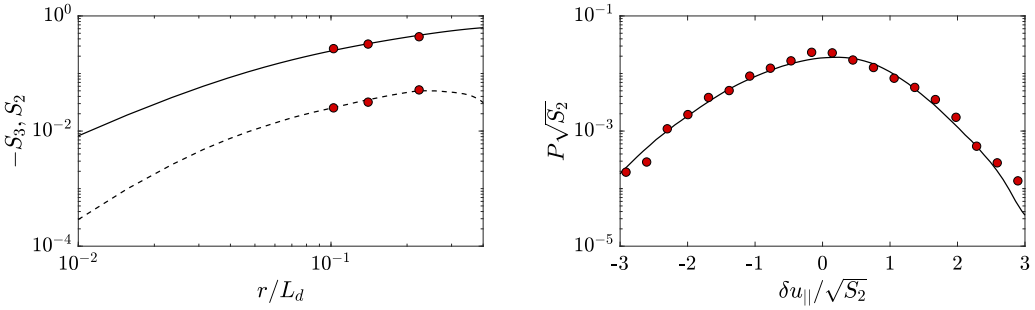

Fig. 17. Left: Second-order S_2 (solid line) and third-order S_3 (dashed line) velocity structure functions computed in the standard Eulerian way and the same measure obtained with the Lagrangian fibre tracking for the $\gamma/\gamma_{crit} = 0.3$ case (blue circles). Right: probability density function (P) of the longitudinal velocity increments $\gamma/\gamma_{crit} = 0.3$. The solid line refers to the Eulerian PDF, while the bullets to the PDF from the Lagrangian fibre measurements.
Source: Adapted from [34].

especially in scenarios where these fibres exhibit significant deformations. This area is particularly relevant for understanding natural processes and in designing engineering applications where flexible fibres are involved.

Secondly, developing and refining measurement techniques using fibre-like objects can open new doors in experimental turbulence research. The potential of these techniques to measure complex flow properties with greater accuracy could lead to breakthroughs in our understanding of turbulence.

Finally, the environmental impact of microplastics and other fibre-like pollutants in aquatic environments remains a pressing concern. Further research in this area is essential for developing effective strategies to address this global challenge.

In conclusion, the study of turbulent flows laden with fibre-like objects is a vibrant and rapidly evolving field. The progress made so far has been substantial, but there remains much to explore and understand. As computational and experimental techniques continue to advance, we can expect even deeper insights into the complex dynamics of these systems.

CRediT authorship contribution statement

Alessandro Chiarini: Writing – review & editing, Writing – original draft. **Marco Edoardo Rosti:** Writing – review & editing, Supervision. **Andrea Mazzino:** Writing – review & editing, Supervision, Conceptualization.

Declaration of competing interest

The authors declare that they have no known competing financial interests or personal relationships that could have appeared to influence the work reported in this paper.

Data availability

No data was used for the research described in the article.

Acknowledgements

M.E.R. was supported by the Okinawa Institute of Science and Technology Graduate University (OIST) with subsidy funding from the Cabinet Office, Government of Japan.

Appendix. List of the works

A non exhaustive list of the references considered in this work are reported in Table A.1. Works dealing with fibre-like object in homogeneous isotropic turbulence and turbulent channel flows are considered. Works based on both numerical simulations and experiments are considered.

Table A.1
Details of some of the references considered in this work dealing with fibre-like objects in homogeneous isotropic turbulence (left) and turbulent channel flow (right). Re_λ is the microscale Reynolds number; L and η denote the length of the fibres and the Kolmogorov scale respectively; ρ_p/ρ_f is the fibre-to-fluid density ratio; Φ_V is the volume fraction of the suspension; Re_τ is the friction Reynolds number; L^+ denotes the length of the fibres in viscous units.

Homogeneous isotropic turbulence						
Ref.	Method	Re_λ	L/η	ρ_p/ρ_f	Φ_V	Type
Shin and Koch [37]	DNS+model	16 – 55	0.3 – 59	≈ 1	$\ll 1$	Rigid
Parsa et al. [41]	Experiment	160 – 214	2.6 – 4.8	≈ 1	$\ll 1$	Rigid
Chevillard and Meneveau [42]	DNS+model	125	< 1	≈ 1	$\ll 1$	Rigid
Byron et al. [44]	DNS+model	435	< 1	≈ 1	$\ll 1$	Rigid
Byron et al. [44]	Experiment	310	10 – 40	1.01	0.1%	Rigid
Parsa and Voth [17]	Experiment	150 – 210	2.8 – 72.9	≈ 1	$\ll 1$	Rigid
Bordoloi and Variano [18]	Experiment	≈ 280	16 – 63	≈ 1	$\ll 1$	Rigid
Bounoua et al. [19]	Experiment	350 – 610	41 – 10^3	≈ 1	$< 0.1\%$	Rigid
Kuperman et al. [36]	Experiment	115	3.6 – 17.3	≈ 1000	$\ll 1$	Rigid
Brizzolara et al. [35]	DNS+IBM	92	20 – 40	$10^2 - 10^3$	$\ll 1$	Rigid
Brizzolara et al. [35]	Experiment	146	90 – 170	≈ 1	$\ll 1$	Rigid
Gay et al. [68]	Experiment	–	250 – 1250	≈ 1	$\ll 1$	Flexible
Olivieri et al. [27]	DNS+IBM	120	4 – 81	1.1 – 10^3	0.003% – 0.6%	Flexible
Rosti et al. [32]	DNS+IBM	92	12 – 25	$10^2 - 10^3$	$\ll 1$	Flexible

(*continued on next page*)

Table A.1 (*continued*).

Turbulent channel flow						
Ref.	Method	Re_τ	L^+	ρ_p/ρ_f	Φ_V	Type
Marchioli et al. [10]	DNS+Model	150	0.75 – 36	$10 - 10^3$	$\ll 1$	Rigid
Do-Quang et al. [22]	DNS+Model	180	3.2 – 24	1 – 1.2	0.1% – 0.4%	Rigid
Shaik et al. [58]	Experiment	435	27.7 – 50.8	1.15	$\ll 1$	Rigid
Shaik and van Hout [59]	Experiment	435	16 – 66.8	1.15 – 1.38	$\ll 1$	Rigid
Baker and Coletti [63]	Experiment	620	50	≈ 1	10^{-4}	Rigid
Alipour et al. [66]	Experiment	360	10	1.15	$\ll 1$	Rigid
Alipour et al. [67]	Experiment	180 – 720	5 – 20	1.15	$\ll 1$	Rigid
Dotto and Marchioli [69]	DNS+Model	150	4 – 12	50 – 3000	$\ll 1$	Flexible
Di Giusto and Marchioli [57]	DNS+Model	150	180	1.3 – 1300	$10^{-4} - 10^{-5}$	Flexible

References

[1] F. Lundell, L.D. Söderberg, P.H. Alfredsson, Fluid mechanics of papermaking, Annu. Rev. Fluid Mech. 43 (2011) 195–217, http://dx.doi.org/10.1146/annurev-fluid-122109-160700.

[2] M.J. Shelley, J. Zhang, Flapping and bending bodies interacting with fluid flows, Annu. Rev. Fluid Mech. 43 (2011) 449–465, http://dx.doi.org/10.1146/annurev-fluid-121108-145456.

[3] A. du Roure, E.N. Nazockdast, M.J. Shelley, Dynamics of flexible fibers in viscous flows and fluids, Annu. Rev. Fluid Mech. 51 (2019) 539–572, http://dx.doi.org/10.1146/annurev-fluid-122316-045153.

[4] A. Cózar, F. Echevarría, J.I. González-Gordillo, X. Irigoien, B. Úbeda, S. Hernández-León, A.T. Palma, S. Navarro, J. García-de Lomas, A. Ruiz, M.L. Fernández-de Puelles, C.M. Duarte, Plastic debris in the open ocean, Proc. Natl. Acad. Sci. 111 (2014) 10239–10244, Publisher: Proceedings of the National Academy of Sciences.

[5] M. Filella, Questions of size and numbers in environmental research on microplastics: methodological and conceptual aspects, Environ. Chem. 12 (2015) 527–538, Publisher: CSIRO PUBLISHING.

[6] C. Brouzet, R. Guiné, M.J. Dalbe, B. Favier, N. Vandenberghe, E. Villermaux, G. Verhille, Laboratory model for plastic fragmentation in the turbulent ocean, Phys. Rev. Fluids 6 (2021) 024601, Publisher: American Physical Society.

[7] M.N. Ardekani, G. Sardina, L. Brandt, L. Karp-Boss, R.N. Bearon, E.A. Variano, Sedimentation of inertia-less prolate spheroids in homogenous isotropic turbulence with application to non-motile phytoplankton, J. Fluid Mech. 831 (2017) 655–674, Publisher: Cambridge University Press.

[8] G. Verhille, S. Moulinet, N. Vandenberghe, M. Adda-Bedia, P. Le Gal, Structure and mechanics of aegagropilae fiber network, Proc. Natl. Acad. Sci. 114 (2017) 4607–4612, Publisher: Proceedings of the National Academy of Sciences.

[9] M. Parsheh, M.L. Brown, C.K. Aidun, On the orientation of stiff fibres suspended in turbulent flow in a planar contraction, J. Fluid Mech. 545 (2005) 245–269, Publisher: Cambridge University Press.

[10] C. Marchioli, M. Fantoni, A. Soldati, Orientation, distribution, and deposition of elongated, inertial fibers in turbulent channel flow, Phys. Fluids 22 (2010) 033301, http://dx.doi.org/10.1063/1.3328874.

[11] S. Bagheri, A. Mazzino, A. Bottaro, Spontaneous symmetry breaking of a hinged flapping filament generates lift, Phys. Rev. Lett. 109 (2012) 154502, http://dx.doi.org/10.1103/PhysRevLett.109.154502, URL: https://link.aps.org/doi/10.1103/PhysRevLett.109.154502.

[12] U. Lācis, N. Brosse, F. Ingremeau, A. Mazzino, F. Lundell, H. Kellay, S. Bagheri, Passive appendages generate drift through symmetry breaking, Nature Commun. 5 (5310) (2014).

[13] U.c.v. Lācis, S. Olivieri, A. Mazzino, S. Bagheri, Passive control of a falling sphere by elliptic-shaped appendages, Phys. Rev. Fluids 2 (2017) 033901, http://dx.doi.org/10.1103/PhysRevFluids.2.033901, URL: https://link.aps.org/doi/10.1103/PhysRevFluids.2.033901.

[14] S. Balachandar, J.K. Eaton, Turbulent Dispersed Multiphase Flow, Annu. Rev. Fluid Mech. 42 (2010) 111–133, http://dx.doi.org/10.1146/annurev.fluid.010908.165243.

[15] L. Brandt, F. Coletti, Particle-laden turbulence: Progress and perspectives, Annu. Rev. Fluid Mech. 54 (2022) 159–189, http://dx.doi.org/10.1146/annurev-fluid-030121-021103.

[16] G.A. Voth, A. Soldati, Anisotropic particles in turbulence, Annu. Rev. Fluid Mech. 49 (2017) 249–276, http://dx.doi.org/10.1146/annurev-fluid-010816-060135.

[17] S. Parsa, G.A. Voth, Inertial range scaling in rotations of long rods in turbulence, Phys. Rev. Lett. 112 (2014) 024501, http://dx.doi.org/10.1103/PhysRevLett.112.024501.

[18] A.D. Bordoloi, E. Variano, Rotational kinematics of large cylindrical particles in turbulence, J. Fluid Mech. 815 (2017) 199–222, Publisher: Cambridge University Press.

[19] S. Bounoua, G. Bouchet, G. Verhille, Tumbling of inertial fibers in turbulence, Phys. Rev. Lett. 121 (2018) 124502, http://dx.doi.org/10.1103/PhysRevLett.121.124502.

[20] G.B. Jeffery, L.N.G. Filon, The motion of ellipsoidal particles immersed in a viscous fluid, Proc. R. Soc. Lond. Ser. A 102 (1922) 161–179, Publisher: Royal Society.

[21] J.E. Butler, B. Snook, Microstructural dynamics and rheology of suspensions of rigid fibers, Annu. Rev. Fluid Mech. 50 (2018) 299–318, http://dx.doi.org/10.1146/annurev-fluid-122316-045144, _eprint.

[22] M. Do-Quang, G. Amberg, G. Brethouwer, A.V. Johansson, Simulation of finite-size fibers in turbulent channel flows, Phys. Rev. E 89 (2014) 013006, Publisher: American Physical Society.

[23] M.N. Ardekani, P. Costa, W.P. Breugem, F. Picano, L. Brandt, Drag reduction in turbulent channel flow laden with finite-size oblate spheroids, J. Fluid Mech. 816 (2017) 43–70, http://dx.doi.org/10.1017/jfm.2017.68.

[24] M.N. Ardekani, L. Brandt, Turbulence modulation in channel flow of finite-size spheroidal particles, J. Fluid Mech. 859 (2019) 887–901, Publisher: Cambridge University Press.

[25] M. Cavaiola, S. Olivieri, A. Mazzino, The assembly of freely moving rigid fibres measures the flow velocity gradient tensor, J. Fluid Mech. 894 (A25) (2020) http://dx.doi.org/10.1017/jfm.2020.288.

[26] S. Olivieri, A. Mazzino, M.E. Rosti, Universal flapping states of elastic fibers in modulated turbulence, Phys. Fluids 33 (2021) 071704, http://dx.doi.org/10.1063/5.0058835.

[27] S. Olivieri, A. Mazzino, M.E. Rosti, On the fully coupled dynamics of flexible fibres dispersed in modulated turbulence, J. Fluid Mech. 946 (A34) (2022b) http://dx.doi.org/10.1017/jfm.2022.611.

[28] Y.N. Young, M.J. Shelley, Stretch-coil transition and transport of fibers in cellular flows, Phys. Rev. Lett. 99 (2007) 058303, Publisher: American Physical Society.

[29] E. Wandersman, N. Quennouz, M. Fermigier, A. Lindner, O.d. Roure, Buckled in translation, Soft Matter 6 (2010) 5715–5719, Publisher: The Royal Society of Chemistry.

[30] N. Quennouz, M. Shelley, O.du. Roure, A. Lindner, Transport and buckling dynamics of an elastic fibre in a viscous cellular flow, J. Fluid Mech. 769 (2015) 387–402, Publisher: Cambridge University Press.

[31] S. Olivieri, I. Cannon, M.E. Rosti, The effect of particle anisotropy on the modulation of turbulent flows, J. Fluid Mech. 950 (R2) (2022a) http://dx.doi.org/10.1017/jfm.2022.832.

[32] M.E. Rosti, A.A. Banaei, L. Brandt, A. Mazzino, Flexible fiber reveals the two-point statistical properties of turbulence, Phys. Rev. Lett. 121 (2018) 044501, http://dx.doi.org/10.1103/PhysRevLett.121.044501.

[33] B. Hejazi, M. Krellenstein, G.A. Voth, Using deformable particles for single-particle measurements of velocity gradient tensors, Exp. Fluids 60 (2019) 153, http://dx.doi.org/10.1007/s00348-019-2796-0.

[34] M.E. Rosti, S. Olivieri, A.A. Banaei, L. Brandt, A. Mazzino, Flowing fibers as a proxy of turbulence statistics, Meccanica 55 (2020) 357–370, http://dx.doi.org/10.1007/s11012-019-00997-2.

[35] S. Brizzolara, M.E. Rosti, S. Olivieri, L. Brandt, M. Holzner, A. Mazzino, Fiber tracking velocimetry for two-point statistics of turbulence, Phys. Rev. X 11 (2021) 031060, http://dx.doi.org/10.1103/PhysRevX.11.031060.

[36] S. Kuperman, L. Sabban, R. van Hout, Inertial effects on the dynamics of rigid heavy fibers in isotropic turbulence, Phys. Rev. Fluids 4 (2019) 064301, http://dx.doi.org/10.1103/PhysRevFluids.4.064301.

[37] M. Shin, D.L. Koch, Rotational and translational dispersion of fibres in isotropic turbulent flows, J. Fluid Mech. 540 (2005) 143–173, http://dx.doi.org/10.1017/S0022112005005690.

[38] G.K. Batchelor, The stress system in a suspension of force-free particles, J. Fluid Mech. 41 (1970) 545–570, http://dx.doi.org/10.1017/S0022112070000745.

[39] S.S. Girimaji, S.B. Pope, Material-element deformation in isotropic turbulence, J. Fluid Mech. 220 (1990) 427–458, Publisher: Cambridge University Press.

[40] G.A. Voth, A.L. Porta, A.M. Crawford, J. Alexander, E. Bodenschatz, Measurement of particle accelerations in fully developed turbulence, J. Fluid Mech. 469 (2002) 121–160, http://dx.doi.org/10.1017/S0022112002001842.

[41] S. Parsa, E. Calzavarini, F. Toschi, G.A. Voth, Rotation rate of rods in turbulent fluid flow, Phys. Rev. Lett. 109 (2012) 134501, http://dx.doi.org/10.1103/PhysRevLett.109.134501.

[42] L. Chevillard, C. Meneveau, Orientation dynamics of small, triaxial–ellipsoidal particles in isotropic turbulence, J. Fluid Mech. 737 (2013) 571–596, http://dx.doi.org/10.1017/jfm.2013.580.

[43] M. Junk, R. Illner, A new derivation of Jeffery's equation, J. Math. Fluid Mech. 9 (2007) 455–488.

[44] M. Byron, J. Einarsson, K. Gustavsson, G. Voth, B. Mehlig, E. Variano, Shape-dependence of particle rotation in isotropic turbulence, Phys. Fluids 27 (2015) 035101, http://dx.doi.org/10.1063/1.4913501.

[45] R. Ni, S. Kramel, N.T. Ouellette, G.A. Voth, Measurements of the coupling between the tumbling of rods and the velocity gradient tensor in turbulence, J. Fluid Mech. 766 (2015) 202–225, http://dx.doi.org/10.1017/jfm.2015.16.

[46] L. Sabban, A. Cohen, R. van Hout, Temporally resolved measurements of heavy, rigid fibre translation and rotation in nearly homogeneous isotropic turbulence, J. Fluid Mech. 814 (2017) 42–68, http://dx.doi.org/10.1017/jfm.2017.12.

[47] G.H. Good, .P.J. Ireland, G.P. Bewley, E. Bodenschatz, L.R. Collins, Z. Warhaft, Settling regimes of inertial particles in isotropic turbulence, J. Fluid Mech. 759 (R3) (2014).

[48] L. Sabban, R. van Hout, Measurements of pollen grain dispersal in still air and stationary, near homogeneous, isotropic turbulence, J. Aerosol Sci. 42 (2011) 867–882, http://dx.doi.org/10.1016/j.jaerosci.2011.08.001, URL: https://www.sciencedirect.com/science/article/pii/S0021850211001352.

[49] M.S. Aswathy, M.E. Rosti, The dynamics of fibres dispersed in viscoelastic turbulent flows, J. Fluid Mech. 984 (A72) (2024).

[50] H. Zhang, G. Ahmadi, F.G. Fan, J.B. McLaughlin, Ellipsoidal particles transport and deposition in turbulent channel flows, Int. J. Multiph. Flow 27 (2001) 971–1009.

[51] J.S. Paschkewitz, Y. Dubief, C.D. Dimitropoulos, E.S.G. Shaqfeh, P. Moin, Numerical simulation of turbulent drag reduction using rigid fibres, J. Fluid Mech. 518 (2004) 281–317, http://dx.doi.org/10.1017/S0022112004001144.

[52] J.S. Paschkewitz, C.D. Dimitropoulos, Y.X. Hou, V.S.R. Somandepalli, M.G. Mungal, E.S.G. Shaqfeh, P. Moin, An experimental and numerical investigation of drag reduction in a turbulent boundary layer using a rigid rodlike polymer, Phys. Fluids 17 (2005) 085101, http://dx.doi.org/10.1063/1.1993307.

[53] J. Andrić, S.T. Fredriksson, S.B. Lindström, S. Sasic, H. Nilsson, A study of a flexible fiber model and its behavior in DNS of turbulent channel flow, Acta Mech. 224 (2013) 2359–2374, http://dx.doi.org/10.1007/s00707-013-0918.

[54] A. Moosaie, M. Manhart, Direct Monte Carlo simulation of turbulent drag reduction by rigid fibers in a channel flow, Acta Mech. 224 (2013) 2385–2413, http://dx.doi.org/10.1007/s00707-013-0919-x.

[55] L. Zhao, N.R. Challabotla, H.I. Andersson, E.A. Variano, Rotation of nonspherical particles in turbulent channel flow, Phys. Rev. Lett. 115 (2015) 244501, Publisher: American Physical Society.

[56] Z. Cui, A. Dubey, L. Zhao, B. Mehlig, Alignment statistics of rods with the Lagrangian stretching direction in a channel flow, J. Fluid Mech. 901 (A16) (2020).

[57] D. Di Giusto, C. Marchioli, Turbulence modulation by slender fibers, Fluids 7 (255) (2022) Number: 8 Publisher: Multidisciplinary Digital Publishing Institute.

[58] S. Shaik, S. Kuperman, V. Rinsky, R. van Hout, Measurements of length effects on the dynamics of rigid fibers in a turbulent channel flow, Phys. Rev. Fluids 5 (2020) 114309, URL: https://link.aps.org/doi/10.1103/PhysRevFluids.5.114309. publisher: American Physical Society.

[59] S. Shaik, R. van Hout, Kinematics of rigid fibers in a turbulent channel flow, Int. J. Multiph. Flow 158 (2023) 104262, http://dx.doi.org/10.1016/j.ijmultiphaseflow.2022.104262.

[60] A. Capone, G.P. Romano, A. Soldati, Experimental investigation on interactions among fluid and rod-like particles in a turbulent pipe jet by means of particle image velocimetry, Exp. Fluids 56 (1) (2014).

[61] A. Capone, G.P. Romano, Interactions between fluid and fibers in a turbulent backward-facing step flow, Phys. Fluids 27 (2015) 053303.

[62] A. Capone, M. Miozzi, G.P. Romano, On translational and rotational relative velocities of fibers and fluid in a turbulent channel flow with a backward-facing step, Int. J. Multiph. Flow 94 (2017) 189–200, http://dx.doi.org/10.1016/j.ijmultiphaseflow.2017.04.021, URL: https://www.sciencedirect.com/science/article/pii/S030193221630684X.

[63] L.J. Baker, F. Coletti, Experimental investigation of inertial fibres and disks in a turbulent boundary layer, J. Fluid Mech. 943 (A27) (2022).

[64] P.H. Mortensen, H.I. Andersson, J.J.J. Gillissen, B.J. Boersma, Dynamics of prolate ellipsoidal particles in a turbulent channel flow, Phys. Fluids 20 (2008) 093302, http://dx.doi.org/10.1063/1.2975209.

[65] J. Jeong, F. Hussain, W. Schoppa, J. Kim, Coherent structures near the wall in a turbulent channel flow, J. Fluid Mech. 332 (1997) 185–214.

[66] M. Alipour, M.D. Paoli, S. Ghaemi, A. Soldati, Long non-axisymmetric fibres in turbulent channel flow, J. Fluid Mech. 916 (A3) (2021).

[67] M. Alipour, M.D. Paoli, A. Soldati, Influence of Reynolds number on the dynamics of rigid, slender and non-axisymmetric fibres in channel flow turbulence, J. Fluid Mech. 934 (2022) A18.

[68] A. Gay, B. Favier, G. Verhille, Characterisation of flexible fibre deformations in turbulence, Europhys. Lett. 123 (2018) 24001, http://dx.doi.org/10.1209/0295-5075/123/24001.

[69] D. Dotto, C. Marchioli, Orientation, distribution, and deformation of inertial flexible fibers in turbulent channel flow, Acta Mech. 230 (2019) 597–621, http://dx.doi.org/10.1007/s00707-018-2355-4.

[70] J.C.H. Fung, J.C.R. Hunt, N.A. Malik, R.J. Perkins, Kinematic simulation of homogeneous turbulence by unsteady random Fourier modes, J. Fluid Mech. 236 (1992) 281–318, Publisher: Cambridge University Press.

[71] W.X. Huang, S.J. Shin, H.J. Sung, Simulation of flexible filaments in a uniform flow by the immersed boundary method, J. Comput. Phys. 226 (2007) 2206–2228, http://dx.doi.org/10.1016/j.jcp.2007.07.002.

[72] J.K. Eaton, J.R. Fessler, Preferential concentration of particles by turbulence, Int. J. Multiph. Flow 20 (1994) 169–209.

[73] S. Allende, C. Henry, J. Bec, Dynamics and fragmentation of small inextensible fibres in turbulence, Phil. Trans. R. Soc. A 378 (2020) 20190398, Publisher: Royal Society.

[74] C.M. White, M.G. Mungal, Mechanics and prediction of turbulent drag reduction with polymer additives, Annu. Rev. Fluid Mech. 40 (2008) 235–256.

[75] R. Benzi, E.S. Ching, Polymers in Fluid Flows, Annu. Rev. Condens. Matter Phys. 9 (2018) 163–181.

[76] S. Takagi, Y. Matsumoto, Surfactant effects on bubble motion and bubbly flows, Annu. Rev. Fluid Mech. 43 (2011) 615–636.

[77] R. Verschoof, R. Van der Veen, C. Sun, D. Lohse, Bubble drag reduction requires large bubbles, Phys. Rev. Lett. 117 (2016) 104502.

[78] J. Gillissen, B. Boersma, P. Mortensen, H. Anderson, Fibre-induced drag reduction, J. Fluid Mech. 602 (2008) 209–218.

[79] C. Marchioli, M. Campolo, Drag reduction in turbulent flows by polymer and fiber additives, KONA Powder Part. J. 38 (2021) 64–81.

[80] O. Forgacs, A. Robertson, S. Mason, The hydrodynamic behaviour of paper-making fibres, Pulp Paper Mag. Can. 59 (1958) 117–128.

[81] J. Randin, E. Yeager, Differential capacitance study on the edge orientation of pyrolytic graphite and glassy carbon electrodes, J. Electroanal. Chem. Interfacial Electrochem. 58 (1975) 313–322, http://dx.doi.org/10.1016/S0022-0728(75)80089-1, URL: https://www.sciencedirect.com/science/article/pii/S0022072875800891.

[82] H. Choi, P. Moin, J. Kim, Active turbulence control for drag reduction in wall-bounded flows, J. Fluid Mech. 262 (1994) 75–110.

[83] D. Gatti, M. Quadrio, Reynolds-number dependence of turbulent skin-friction drag reduction induced by spanwise forcing, J. Fluid Mech. 802 (2016) 553–558.

[84] J. Jiménez, A. Pinelli, The autonomous cycle of near-wall turbulence, J. Fluid Mech. 389 (1999) 335–359, http://dx.doi.org/10.1017/S0022112099005066.

[85] P. Gualtieri, F. Picano, G. Sardina, C.M. Casciola, Exact regularized point particle method for multiphase flows in the two-way coupling regime, J. Fluid Mech. 773 (2015) 520–561.

[86] F. Picano, W.P. Breugem, L. Brandt, Turbulent channel flow of dense suspensions of neutrally buoyant spheres, J. Fluid Mech. 764 (2015) 463–487, http://dx.doi.org/10.1017/jfm.2014.704.

[87] P. Costa, F. Picano, L. Brandt, W.P. Breugem, Universal scaling laws for dense particle suspensions in turbulent wall-bounded flows, Phys. Rev. Lett. 117 (2016) 134501, http://dx.doi.org/10.1103/PhysRevLett.117.134501.

[88] W. Fornari, A. Formenti, F. Picano, L. Brandt, The effect of particle density in turbulent channel flow laden with finite size particles in semi-dilute conditions, Phys. Fluids 28 (2016) 033301, http://dx.doi.org/10.1063/1.4942518.

[89] M.N. Ardekani, P. Costa, W.P. Breugem, L. Brandt, Numerical study of the sedimentation of spheroidal particles, Int. J. Multiph. Flow 87 (2016) 16–34.

[90] R.J. Adrian, Particle-imaging techniques for experimental fluid mechanics, Annu. Rev. Fluid Mech. 23 (1991) 261–304, http://dx.doi.org/10.1146/annurev.fl.23.010191.001401.

[91] T. Dombre, U. Frisch, J.M. Greene, M. Hénon, A. Mehr, A.M. Soward, Chaotic streamlines in the ABC flows, J. Fluid Mech. 167 (1986) 353–391, http://dx.doi.org/10.1017/S0022112086002859.

[92] M. Cavaiola, A. Mazzino, Self-propelled slender objects can measure flow signals net of self-motion, Phys. Fluids 33 (2021) 053603, http://dx.doi.org/10.1063/5.0051325.

[93] L. Richardson, Atmospheric diffusion shown on a distance-neighbour graph, Proc. R. Soc. A 110 (1926) 709–737.

[94] S. Kramel, G.A. Voth, S. Tympel, F. Toschi, Preferential rotation of chiral dipoles in isotropic turbulence, Phys. Rev. Lett. 117 (2016) 154501, http://dx.doi.org/10.1103/PhysRevLett.117.154501.

[95] R. Ni, N.T. Ouellette, G.A. Voth, Alignment of vorticity and rods with Lagrangian fluid stretching in turbulence, J. Fluid Mech. 743 (R3) (2014) http://dx.doi.org/10.1017/jfm.2014.32.

[96] C. Brouzet, G. Verhille, P. Le Gal, Flexible fiber in a turbulent flow: A macroscopic polymer, Phys. Rev. Lett. 112 (2014) 074501, http://dx.doi.org/10.1103/PhysRevLett.112.074501.

[97] G. Verhille, A. Bartoli, 3D conformation of a flexible fiber in a turbulent flow, Exp. Fluids 57 (2016) 117, http://dx.doi.org/10.1007/s00348-016-2201-1.